

Accepted Manuscript



Regional unit definition for the nucleus of comet 67P/Churyumov-Gerasimenko on the SHAP7 model

N. Thomas, M.R. El Maarry, P. Theologou, F. Preusker, F. Scholten, L. Jorda, S.F. Hviid, R. Marschall, E. Kührt, G. Naletto, H. Sierks, P.L. Lamy, R. Rodrigo, D. Koschny, B. Davidsson, M.A. Barucci, J.L. Bertaux, I. Bertini, D. Bodewits, G. Cremonese, V. Da Deppo, S. Debei, M. De Cecco, S. Fornasier, M. Fulle, O. Groussin, P.J. Gutiérrez, C. Güttler, W.H. Ip, H.U. Keller, J. Knollenberg, L.M. Lara, M. Lazzarin, J.J. López-Moreno, F. Marzari, C. Tubiana, J.B. Vincent

PII: S0032-0633(18)30069-2

DOI: [10.1016/j.pss.2018.05.019](https://doi.org/10.1016/j.pss.2018.05.019)

Reference: PSS 4549

To appear in: *Planetary and Space Science*

Received Date: 18 February 2018

Revised Date: 20 April 2018

Accepted Date: 31 May 2018

Please cite this article as: Thomas, N., El Maarry, M.R., Theologou, P., Preusker, F., Scholten, F., Jorda, L., Hviid, S.F., Marschall, R., Kührt, E., Naletto, G., Sierks, H., Lamy, P.L., Rodrigo, R., Koschny, D., Davidsson, B., Barucci, M.A., Bertaux, J.L., Bertini, I., Bodewits, D., Cremonese, G., Da Deppo, V., Debei, S., De Cecco, M., Fornasier, S., Fulle, M., Groussin, O., Gutiérrez, P.J., Güttler, C., Ip, W.H., Keller, H.U., Knollenberg, J., Lara, L.M., Lazzarin, M., López-Moreno, J.J., Marzari, F., Tubiana, C., Vincent, J.B., Regional unit definition for the nucleus of comet 67P/Churyumov-Gerasimenko on the SHAP7 model, *Planetary and Space Science* (2018), doi: 10.1016/j.pss.2018.05.019.

This is a PDF file of an unedited manuscript that has been accepted for publication. As a service to our customers we are providing this early version of the manuscript. The manuscript will undergo copyediting, typesetting, and review of the resulting proof before it is published in its final form. Please note that during the production process errors may be discovered which could affect the content, and all legal disclaimers that apply to the journal pertain.

Regional unit definition for the nucleus of comet

67P/Churyumov-Gerasimenko on the SHAP7 model

N. Thomas¹, M.R. El Maarry², P. Theologou¹, F. Preusker³, F. Scholten³, L. Jorda⁴, S.F. Hviid³, R. Marschall^{1,5}, E. Kührt³, G. Naletto^{6,7,8}, H. Sierks⁹, P. L. Lamy⁴, R. Rodrigo^{10,11}, D. Koschny¹², B. Davidsson¹³, M. A. Barucci¹⁴, J.-L. Bertaux¹⁵, I. Bertini¹⁶, D. Bodewits¹⁷, G. Cremonese¹⁸, V. Da Deppo⁸, S. Debei¹⁹, M. De Cecco²⁰, S. Fornasier¹⁴, M. Fulle²¹, O. Groussin²², P. J. Gutiérrez²³, C. Güttler⁹, W.-H. Ip^{24,25}, H. U. Keller^{3,26}, J. Knollenberg³, L. M. Lara²³, M. Lazzarin¹⁶, J. J. Lòpez-Moreno²³, F. Marzari⁶, C. Tubiana⁹, J.-B. Vincent³

¹Physikalisches Institut, Sidlerstr. 5, University of Bern, CH-3012 Bern, SWITZERLAND.

²Laboratory for Atmospheric and Space Physics, University of Colorado, 3665 Discovery Drive, CO 80301, USA.

³Deutsches Zentrum für Luft- und Raumfahrt (DLR), Institut für Planetenforschung, Asteroiden und Kometen, Rutherfordstraße 2, 12489 Berlin, Germany

⁴Laboratoire d'Astrophysique de Marseille, 38 Rue de Frédéric Joliot-Curie, 13388 Marseille Cedex 13, France

⁵International Space Science Institute, Hallerstraße 6, 3012 Bern, Switzerland.

⁶University of Padova, Department of Physics and Astronomy "Galileo Galilei", Via Marzolo 8, 35131 Padova, Italy

⁷University of Padova, Center of Studies and Activities for Space (CISAS) "G. Colombo", Via Venezia 15, 35131 Padova, Italy

⁸CNR-IFN UOS Padova LUXOR, Via Trasea 7, 35131 Padova, Italy

⁹Max Planck Institute for Solar System Research, Justus-von-Liebig-Weg 3, 37077 Göttingen, Germany

¹⁰Centro de Astrobiología, CSIC-INTA, 28850 Torrejon de Ardoz, Madrid, Spain

¹¹International Space Science Institute, Hallerstrasse 6, 3012 Bern, Switzerland

¹²Scientific Support Office, European Space Research and Technology Centre/ESA, Keplerlaan 1, Postbus 299, 2201 AZ Noordwijk ZH, The Netherlands

¹³Jet Propulsion Laboratory, M/S 183-401, 4800 Oak Grove Drive, Pasadena, CA 91109, USA

¹⁴LESIA, Observatoire de Paris, Université PSL, CNRS, Univ. Paris Diderot, Sorbonne Paris Cité, Sorbonne Université, 5 place Jules Janssen, 92195 Meudon, France

¹⁵LATMOS, CNRS/UVSQ/IPSL, 11 Boulevard d'Alembert, 78280 Guyancourt, France

- ¹⁶University of Padova, Department of Physics and Astronomy "Galileo Galilei", Vicolo dell'Osservatorio 3, 35122 Padova, Italy
- ¹⁷Department of Astronomy, University of Maryland, College Park, MD 20742-2421, USA
- ¹⁸INAF, Astronomical Observatory of Padova, Vicolo dell'Osservatorio 5, 35122 Padova, Italy
- ¹⁹University of Padova, Department of Industrial Engineering, Via Venezia 1, 35131 Padova, Italy
- ²⁰University of Trento, Faculty of Engineering, Via Mesiano 77, 38121 Trento, Italy
- ²¹INAF Astronomical Observatory of Trieste, Via Tiepolo 11, 34143 Trieste, Italy
- ²²Aix Marseille Université, CNRS, LAM (Laboratoire d'Astrophysique de Marseille) UMR 7326, 13388 Marseille, France
- ²³Instituto de Astrofísica de Andalucía (CSIC), c/ Glorieta de la Astronomía s/n, 18008 Granada, Spain
- ²⁴Graduate Institute of Astronomy, National Central University, 300 Chung-Da Rd, Chung-Li 32054, Taiwan
- ²⁵Space Science Institute, Macau University of Science and Technology, Avenida Wai Long, Taipa, Macau
- ²⁶Institut für Geophysik und extraterrestrische Physik, Technische Universität Braunschweig, Mendelssohnstr. 3, 38106 Braunschweig, Germany

*Correspondence to: Nicolas Thomas, Physikalisches Institut, Sidlerstrasse 5, University of Bern, 3012, Bern, Switzerland. (nicolas.thomas@space.unibe.ch) Tel: +41 31 631 4406

Address for correspondence:

N. Thomas
Physikalisches Institut
Sidlerstrasse 5,
CH-3012 Bern,
SWITZERLAND.
Tel: [41]-31-631-4406
E-mail: nicolas.thomas@space.unibe.ch

Prepared for submission to: Planetary and Space Science

Running head: Regions on 67P

Subject headings:

This manuscript contains:

Pages	34 (single spaced)
Figures	24
Tables	2
References	15

April 14, 2018

1 Regional unit definition for the nucleus of comet 67P/Churyumov-Gerasimenko on the SHAP7 model
2
3 N. Thomas¹, M.R. El Maarry², P. Theologou¹, F. Preusker³, F. Scholten³, L. Jorda⁴, S.F.
4 Hviid³, R. Marschall^{1,5}, E. Kührt³, G. Naletto^{6,7,8},
5
6 H. Sierks⁹, P. L. Lamy⁴, R. Rodrigo^{10,11}, D. Koschny¹², B. Davidsson¹³, M. A. Barucci¹⁴, J.-L.
7 Bertaux¹⁵, I. Bertini¹⁶, D. Bodewits¹⁷, G. Cremonese¹⁸, V. Da Deppo⁸, S. Debei¹⁹, M. De
8 Cecco²⁰, S. Fornasier¹⁴, M. Fulle²¹, O. Groussin²², P. J. Gutiérrez²³, C. Güttler⁹, W.-H. Ip^{24,25},
9 H. U. Keller^{3,26}, J. Knollenberg³, L. M. Lara²³, M. Lazzarin¹⁶, J. J. López-Moreno²³, F.
10 Marzari⁶, C. Tubiana⁹, J.-B. Vincent³
11
12
13
14

15 **Abstract**

16 The previously defined regions on the nucleus of comet 67P/Churyumov-Gerasimenko have been
17 mapped back onto the 3D SHAP7 model of the nucleus (Preusker et al., 2017). The resulting regional
18 definition is therefore self-consistent with boundaries that are well defined in 3 dimensions. The
19 facets belonging to each region are provided as supplementary material. The shape model has then
20 been used to assess inhomogeneity of nucleus surface morphology within individual regions. Several
21 regions show diverse morphology. We propose sub-division of these regions into clearly identifiable
22 units (sub-regions) and a comprehensive table is provided. The surface areas of each sub-region
23 have been computed and statistics based on grouping of unit types are provided. The roughness of
24 each region is also provided in a quantitative manner using a technique derived from computer
25 graphics applications. The quantitative method supports the sub-region definition by showing that
26 differences between sub-regions can be numerically justified.

27 **Key words:** Rosetta, 67P/Churyumov-Gerasimenko, nucleus, morphology
28

29 **1. Introduction**

30 Observations of the nucleus of 67P/Churyumov-Gerasimenko (hereafter 67P) by the OSIRIS
31 imaging system (Keller et al., 2007) from onboard the European Space Agency's Rosetta spacecraft
32 revealed a bi-lobate object (Sierks et al., 2015) with diverse surface morphology (Thomas et al.,
33 2015). The shape of the nucleus has been refined in several steps (e.g. Preusker et al., 2015; 2017;
34 Jorda et al., 2015) and has now reached metre-scale accuracy over most of the object. 67P can be
35 crudely separated into a roundish "head" representing the smaller lobe of 2.50 km x 2.14 km x 1.64
36 km (Jorda et al., 2016) and an ellipsoidal "body" representing the larger lobe of 4.10 km x 3.52 km x
37 1.63 km in dimension. The two lobes are linked by a thin, narrow, "neck" that corresponds to around
38 7% of the total volume.

39 The surface morphology was used to define regions in the northern hemisphere by Thomas et al.
40 (2015) and El-Maarry et al. (2015). These regions were intended to group areas with common
41 properties not merely for reasons of nomenclature but also for developing relationships between
42 surface morphology and outgassing properties. This was extended to the southern hemisphere by El-
43 Maarry et al. (2016).

44 The irregular shape of the nucleus produced significant self-shadowing. This led to difficulties in
45 tracing regional boundaries in some areas. The neck in the southern hemisphere, for example, could
46 only be observed for a short period because of both the orbit of the comet and the need for Rosetta
47 to remain safe from the effects of reflected light from dust on its star trackers. Hence, some
48 ambiguity arose. Furthermore, analysis of 2D images to produce the boundaries is not simple on
49 such an irregular object. The shape model brings in the third dimension and use of computer tools to
50 view the nucleus from several directions almost simultaneously gives a much clearer vision of the
51 constituent parts of the nucleus. It is also forced to be consistent at boundaries which is something
52 that is not guaranteed when using 2D definitions. We have used this approach to look at the regions
53 individually and thereby identify sub-regions – separating regions where the properties are not
54 uniform across their surfaces.

55 The approach has been to combine 2D global and local images with the shape model to define
56 sub-regional boundaries. This has also allowed us to look at large dust-covered regions (such as Ash
57 and Maat) to obtain a better understanding of the uniformity of the substrate under the dust under
58 the assumption that the dust coverage provided a conformal coating of the surface.

59 In section 2, we shall look at the regions individually and, using both the shape model and 2D
60 images from OSIRIS, attempt to isolate areas with common properties at approximately the square
61 kilometre scale. In section 3, we shall look at some derived products. We can use the surface areas
62 to define percentage coverage of specific morphologies. The surface roughness in the individual
63 regions can also be calculated to give a more quantitative assessment of the surface morphology. In
64 section 4, we provide some straightforward conclusions.

65 **2. The regional definition**

66 **a. Regions on SHAP7**

67 The regions on the nucleus of 67P as defined by Thomas et al. (2015) for the northern
68 hemisphere and El-Maarry et al. (2016) for the southern hemisphere are shown in Figure 1. The
69 montage of 4 different views uses the SHAP7 model of the nucleus (Preusker et al., 2017). The

70 previous works used 2D imaging of the nucleus to support the determination of topographical and
71 morphological boundaries. These were transposed onto the 3D shape model to produce Figure 1.

72 A key aspect of this work is whether an independent person would reach similar conclusions in
73 defining unit boundaries. Using the 3D model, there are three boundaries on 67P where an
74 improved definition could be foreseen.

75 The area around the interfaces between Hapi, Sobek, Neith, Hathor, and Bastet is a good
76 example. In this area, the neck is narrow between Aker on the body side and Bastet/Hathor on the
77 head side. Hapi is smooth and dust covered whereas Aker is rocky in appearance but also relatively
78 smooth. The difficulty arises from where the rough terrain of Sobek and Neith meets the rough
79 terrain of Bastet and Hathor. The extent to which a common unit extends into the neck is uncertain.

80 The 3D shape model suggests an alternative interpretation of the boundary between Geb, Bes,
81 and Anhur. It can be seen in 3D that part of Anhur extends upwards onto a plateau that could be
82 defined as part of Bes. This suggest that this sub-region was originally misclassified because of the
83 lack of observations and a detailed shape model in 2015. We shall address this below in defining
84 sub-regions.

85 Finally, the Khepry region has two major components that are almost orthogonal to each other
86 when mapped onto the shape model. This is potentially misleading and could be re-defined. Again,
87 we address this below in defining sub-regions.

88 Our philosophy throughout is to maintain the previous nomenclature as the number of possible
89 misclassifications is rather small but to identify possible reclassification by using the sub-region
90 definition.

91 The full sub-region definition is provided in the form of a table (Table 1) and provides 71
92 separate sub-regions. We refer to this sub-region nomenclature in this table throughout.

93 **Table 1 Each region is sub-divided (where feasible) into sub-regions. The surface area of each region is given and the**
94 **totals for the head, neck and body regions are also shown. The characteristics of the region and of the sub-regions are**
95 **given in each case. We also include unique abbreviations for each region to simplify display.**

Region	Characteristics and Area [km ²]	
Atum (Am)	Complex region with consolidated material and very rough.	
	Sub-region a	A very rough topographic high (with respect to its surroundings) with boulders and some lineaments.
	Sub-region b	A smooth fractured surface adjoining Khonsu. On the Khonsu side, there is a cliff leading to rough fractured terrains possibly indicating loss of this smooth layer. It is topographically at slightly higher elevation than the adjoining Anubis region with a distinct step evident at the boundary.
	Sub-region c	An undulating terrain with intermediate roughness. It is bounded by Anubis and Anhur on the north and south side respectively and by a steep cliff to the east that forms the Geb region.
Khonsu (Kn)	Complex region with a mixture of smooth and rough terrains.	
	Sub-region a	This sub-region is at an angle with respect to the rest of

		the region. It also contains small scale roughness and a lot of boulders.
	Sub-region b	Very rough terrain on many scales adjoining the Apis "face" and showing the side of the rougher part of Atum.
	Sub-region c	Very rough and in places pitted terrain with fractures. Topographically low compared to adjacent Atum sub-regions.
	Sub-region d	Adjoining Atum, this region is very complex. There are flatter areas (dust deposits) but with rough outcrops.
	Sub-region e	A small sub-region which is dominated by flat, apparently dusty material
Apis (Ap)	Consolidated and fractured but topographically smooth. Topographically stands out above Ash	
		0.39798
Imhotep (Im)	Smooth "dusty" depression surrounded by more consolidated material. Circular features at the edges of the smooth terrain	
		4.90446
	Sub-region a	Smooth material at the centre of the region. Observed to change dramatically over the mission. Bounded by Ash to the north. On two sides there are steps upwards to rougher terrain (sub-region b) while on the remaining side there are layers downwards to sub-region c with a more gradual transition than elsewhere.
	Sub-region b	Rim of sub-region a. Contains layered terrain incorporating a large circular structure.
	Sub-region c	Rougher terrain inside the rim of Imhotep. Includes all the small quasi-circular structures. Adjoins the smooth terrain. At the boundary there are indications of layering.
	Sub-region d	Clearly rocky at its edge but covered with smooth material in depressions. Evidence of surface changes in places similar to those observed in sub-region a. Boundary to smooth surface (sub-region a) often associated with a clear scarp. Similar to Khepry although topographically lower.
Anubis (Ab)	Smooth surface probably not consolidated and has undergone surface modification possibly similar to that observed in Imhotep.	
		0.92241
Bes (Be)	Multiply-layered terrain bordering the scarp into the southern part of the neck.	
		2.42084
	Sub-region a	Topographically lowest level. Covered in boulders in some places.
	Sub-region b	Separated from a by a cliff. Contains a diamond-shaped structure surrounding a surface with large boulders
	Sub-region c	Adjoins Imhotep and appears to be at a level intermediate between sub-regions a and b although it has no contact with a. Generally smooth with no major topographic features.
	Sub-region d	A steep cliff separates this level from sub-region c. It is at a higher topographic level – similar to b or possibly slightly higher.
	Sub-region e	The uppermost level. Separated from d by a significant

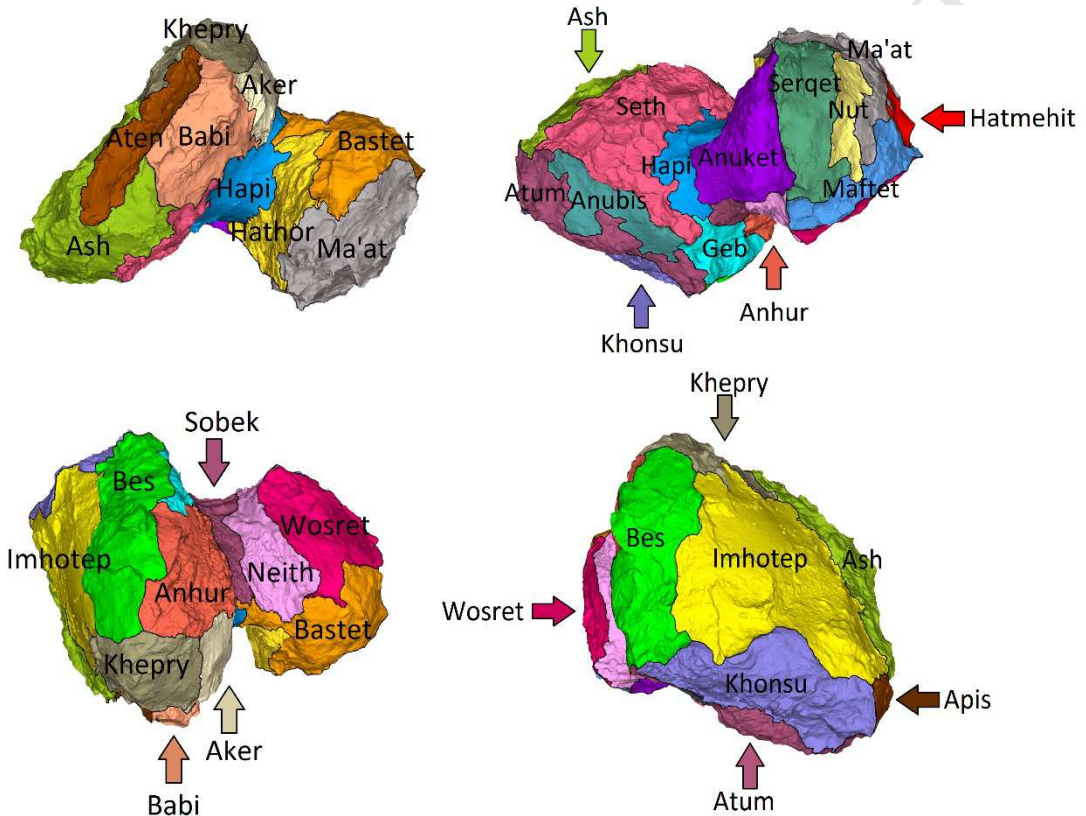
		change in slope. The steep cliff down to Anhur sub-region c is strongly apparent in the shape model.
Seth (Se)	Consolidated, possibly more brittle in nature when compared to other more strongly consolidated regions. Dominated by circular and semi-circular structures and talus..	4.66022
Ash (As)	Covered with a presumed sedimentary deposit producing smooth surface. Occasional exposures of more consolidated but brittle material below.	
	Sub-region a	Adjoining Babi at an edge and the Aten depression via a sharp change in slope, this sub-region adjoins an adjacent sub-region at a rough hummocky interface. The sub-region is mostly smooth with some smaller depressions and small cliffs covered in dust.
	Sub-region b	Adjoining Seth, this sub-region is smooth. Its boundary to Seth is characterized by a transition to rougher terrain and a substantial change in slope.
	Sub-region c	Adjoining Aten, this is rougher terrain. It is topographically higher than sub-region b and where it meets sub-region b there are arc-shaped cliffs.
	Sub-region d	Dust coated. Smoother region.
	Sub-region e	Sub-region containing the large circular structure which may be the result of impact. Possibly related material outside the putative rim is included.
	Sub-region f	Smooth sub-region with a small pit and some scarps. Intermediate in character.
	Sub-region g	Seth like. Adjoining Atum.
	Sub-region h	Adjoining Apis. Rock-like surface with a slight depression. Topographically separated from the rest.
	Sub-region i	Large-scale rough terrain. Dust covered but with exposed layering in many places. Transitions to the Imhotep region at a boundary between very rough terrain and that of intermediate character.
	Sub-region j	Borders Aten and is also a depression but not as deep as Aten. There is a ridge dividing two sections of the sub-region. The bases of the depression on both sides of the ridge are smooth.
Aten (An)	Depression with little or no sedimentary deposits. Interior mainly dominated by talus resulting from progressive rim failure.	1.12758
Babi (Bb)	Covered with a deposit producing a smooth surface. Occasional exposures of more consolidated but brittle material below. Topographically separated from Ash.	
	Sub-region a	Topographic high with cliffs on 3 sides. Uppermost surface is dust covered.
	Sub-region b	Topographically low and strongly sloping. Bounded by Kheptry, Seth and Ash. Some spur-like structures possibly originating from sub-region a are evident.
Geb (Gb)	Consolidated material	
	Sub-region a	Large numbers of depressions on a steep slope.
	Sub-region b	The neck side of Geb. Covered in boulders.

	Sub-region c	Smoother fractured surface similar to that seen in Anhur and Bes.	
Khepry (Kp)	Consolidated and fractured material but rather smooth with ponded deposits.		1.63087
	Sub-region a	Flat but rocky-like sub-region with ponded deposits	
	Sub-region b	A small sub-region with a prominent cliff. Adjoins Bes with similar characteristics.	
	Sub-region c	Topographically almost at right-angles to sub-region a. Highly complex sub-region with rough, rocky terrain, smoother coatings it places and boulders. Talus from collapse of material from Ash is also evident.	
Anhur (Ah)	Consolidated material with significant intermediate scale roughness		1.87013
	Sub-region a	Plateau with extreme intermediate roughness including isolated ridges. Includes some pits.	
	Sub-region b	Cliffs descending from sub-region a to the neck. Surface texture similar to that in sub-region a.	
	Sub-region c	With respect to the roughly ellipsoidal shape of the body, topographically on same level as Bes sub-region a which it adjoins but with the face being at a large angle to Bes sub-region a.	
Aker (Ar)	Strongly consolidated material similar to the adjacent region, Khepry. Contains a large complex fracture system near a steep topographic slope that descends towards Hapi. It has four distinct faces.		0.87022
	Sub-region a	Contains a large set of tectonic fractures and a smooth bottomed shallow depression.	
	Sub-region b	Topographically distinct from sub-region a but has some similarities. It adjoins Anhur where there is a change in slope and surface roughness.	
	Sub-region c	Comprises a cliff that drops sharply to the boundary with Babi at its base. Significant evidence of collapse is evident along the face.	
	Sub-region d	Interfaces primarily with Hapi and is a steep fractured cliff.	
TOTAL BODY			31.66
Hapi (Hp)	Smooth, probably non-consolidated surface		1.98356
Sobek (So)	Consolidated material, texturally very rough		0.83735
	Sub-region a	Set of quasi-parallel steps/small scarps	
	Sub-region b	Boulder-covered terrain	
TOTAL NECK			2.82
Anuket (Ak)	Consolidated, "rocky" appearance. Smooth on large scale but with some large knobs and significant small scale roughness.		2.0523
Neith (Ne)	Mainly comprising the cliff separating Wosret and Sobek. Significant intermediate scale roughness covering the whole region.		1.60746
Maftet (Mf)	Weakly consolidated material dominated by arcuate-shaped depressions and associated talus.		0.67813

Serqet (Sq)	Mix of strongly consolidated material with substantial vertical relief and a smoother dusty deposit area at the base of a cliff.		1.03333
	Sub-region a	Vertical fractured cliff adjoining Anuket	
	Sub-region b	Flat dust covered surface with ripples possibly of gas driven origin adjoining Nut.	
	Sub-region c	Transitional sub-region with rocky material becoming increasingly similar to Maftet-like morphology at the Maftet boundary.	
Nut (Nu)	Depression possibly similar to Aten but significantly shallower.		0.47264
Wosret (Wr)	Consolidated material that appears highly fractured with occasional pits		2.35911
	Sub-region a	An apparently flat "face" with ponded materials and knobby textured terrain.	
	Sub-region b	Topographically lower than sub-region a and displaying long fracture systems.	
	Sub-region c	Rougher terrain with numerous quasi-circular structures and non-aligned ridges and pits.	
Ma'at (Ma)	Covered with a deposit producing a smooth surface on small scales. Occasional exposures of more consolidated but brittle material below. Similar to Ash but with some pits.		3.81651
	Sub-region a	Smooth dust-covered shallow depression with knobs	
	Sub-region b	Smooth dust-covered shallow depression with knobs and an irregular-shaped ridge-like structure at its centre.	
	Sub-region c	Topographically lower with significant numbers of depressions and quasi-circular/arcuate depressions.	
	Sub-region d	A plateau at a lower elevation than Ma'at sub-regions around it. Bounds Bastet at a cliff.	
	Sub-region e	Large-scale roughness dominated substrate with dust-covering.	
Bastet (Bs)	Consolidated material with texturally rough surface and limited amounts of dust coating.		1.98781
	Sub-region a	Smoother terrain adjoining Hatmehit and Wosret.	
	Sub-region b	Undulating terrain on a face at an angle with respect to a. Pock-marked in places.	
	Sub-region c	Fractured consolidation terrain. Parts of this sub-region show similarity to Hathor which adjoins it.	
Hathor (Hh)	Consolidated, but fractured material on a gravitationally steep slope. Comprises most of the cliff separating Ma'at and Hapi.		2.16217
Hatmehit (Hm)	Large circular depression with a smooth interior (some rocks) surrounded by more consolidated material at the rim.		1.08561
	Sub-region a	The floor of the circular depression. This is generally smooth and flat with a small ridge running roughly through the centre. Some talus from fracturing is evident at the margins.	
	Sub-region b	The south and west sides of the rim of the depression adjoining Maftet and Wosret. Contains quasi-circular	

		depressions. The rim of Hatmehit is less pronounced.
	Sub-region c	The north and east sides of the rim of Hatmehit adjoining Bastet and Maat. The steepest parts of the rim are included in this sub-region. The interior of the rim is fractured in many places.
TOTAL HEAD		17.26

96



97

98 **Figure 1** Montage of 4 orientations of the nucleus of 67P showing the region definitions (Thomas et al., 2015; El-
 99 Maarry et al., 2015;2016) on the SHAP7 model.

100 ***b. Regions and evidence of internal units***

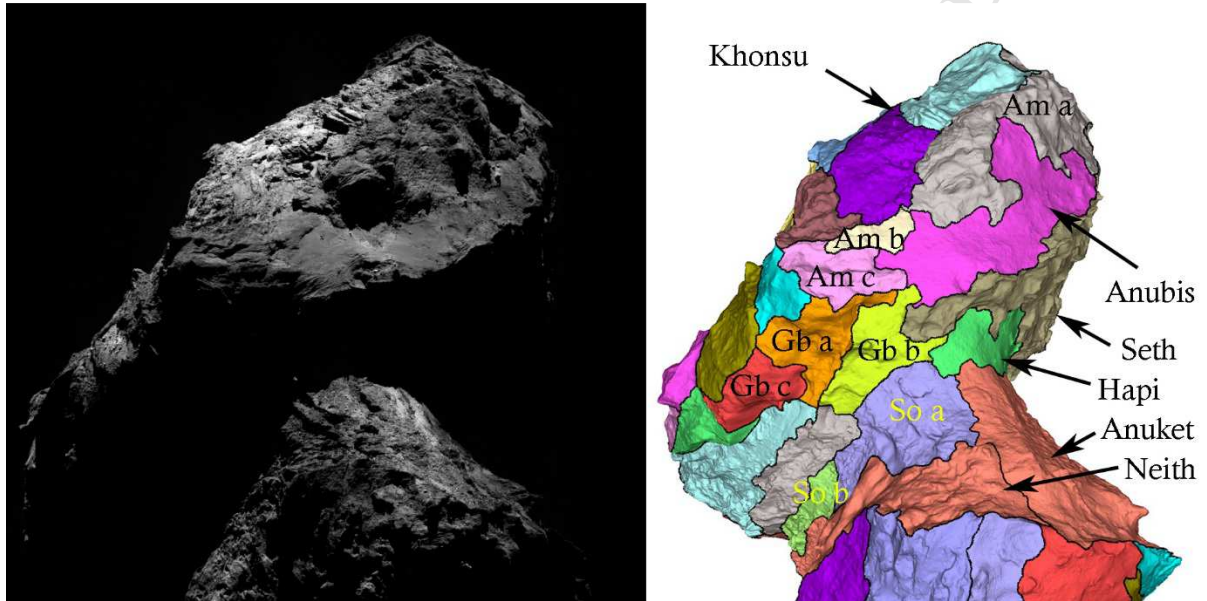
101 ***i. Body***

102 ***1. Atum (Am) and Anubis (Ab)***

103 Atum is a complex region that was close to the terminator in most images during the early phase
 104 of the mission. It can now be seen to have 3 distinct sub-regions. The largest sub-region (sub-region
 105 a in grey in Figure 2 left) is a very rough, topographically high, structure bounded by Anubis to the
 106 north (pink) and Khonsu to the south (violet). The cliff down to Khonsu is steep. The border with
 107 Anubis is gradual.

108 In the regional definition, this sub-region was originally linked to further rough terrain (light pink
 109 in Figure 2 right) via a thin “bridge”. It can be seen in Figure 2 left that the bridge (cream coloured in
 110 Figure 2) is smooth but topographically slightly higher than the Anubis plains material. High
 111 resolution data show it to be fractured. There is a steep cliff downwards to Khonsu on the south
 112 side. For the sub-region definition, the cream region is referred to Atum sub-region b. The remaining
 113 terrain is undulating with intermediate roughness. This is sub-region c.

114 There appear to be no large variations in morphology across Anubis and hence there are no sub-
 115 regions defined. The region showed some surface changes during the mission (El-Maarry et al.,
 116 2017) akin to scarp retreats. The changes appeared to be similar to those seen in the smooth central
 117 part of Imhotep and some parts of Hapi (quasi-circular depressions forming in smooth terrain).
 118



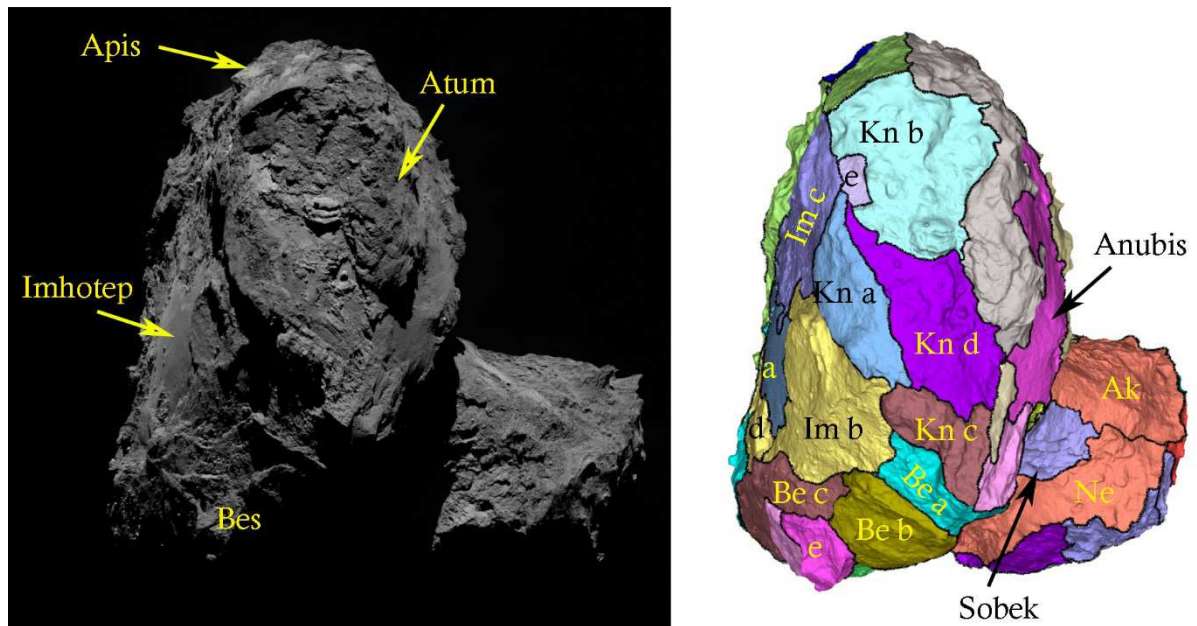
119 Figure 2 Left: OSIRIS image (NAC_2015-12-10T05.01.06.778Z_ID10_1397549000_F22) showing the Anubis-Atum-
 120 Khonsu face on the body and the Anuket-Neith-Sobek section on the head. Right: The regional definition on the shape
 121 model with sub-regions added in the same orientation as the image.
 122

123

124 2. Khonsu (Kn) and Apis (Ap)

125 The Khonsu region was first defined after equinox and is a highly complex region with significant
 126 evidence of surface changes probably produced by activity (El Maarry et al., 2017). Changes in
 127 surface morphology over small scales are evident. A highly detailed definition would result in a large
 128 number of sub-regions. Here, we restrict the definition to 5 main sub-regions.

129 Sub-region a (Figure 3 light blue) is inclined with respect to the rest of the region although the
 130 change in orientation is smooth and not cliff-like. This is evident in Figure 3 left from the change in
 131 reflectance. It also contains small scale roughness and a lot of boulders. It is bounded by the
 132 Imhotep region close to the large quasi-circular structure (yellow in Figure 3 right).
 133



134
135
136 Figure 3 Left: The Khonsu face of the nucleus (NAC_2015-05-02T15.09.20.389Z_ID10_1397549000_F23). Right: The sub-region definition of Khonsu.

137

138 Sub-region b is very rough terrain on many scales. It adjoins the Apis “face” (green in Figure 3
139 right) and has a very sharp boundary defined by the top of a cliff. The north boundary is defined by
140 Atum (sub-region a). The terrain here is probably related to the material making up the elevated
141 topography of Atum. This rougher terrain is evident in Figure 3 left and there is a change in
142 reflectance within the Khonsu region indicating an internal sub-region boundary.

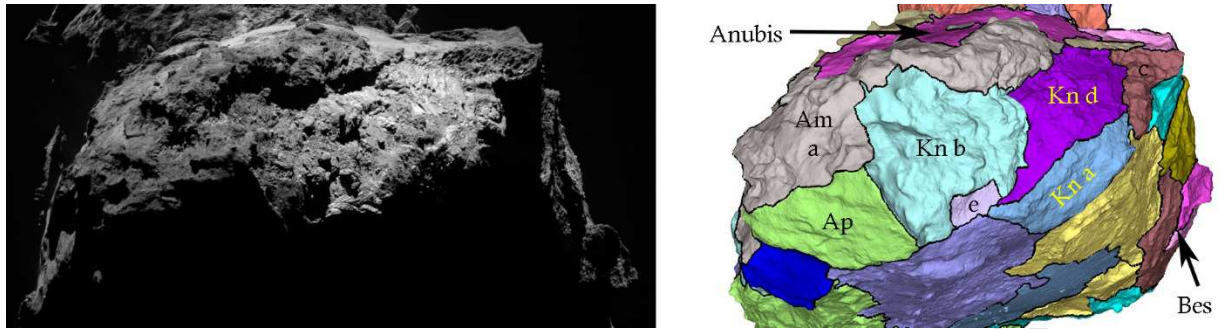
143 Sub-region d is bounded by Atum to the north. It is possibly the most complex sub-region on the
144 nucleus with highly varied terrain types (smooth, boulder covered, aligned lineaments etc.). It is
145 deserving of a detailed sub-regional mapping which is unfortunately beyond the scope here. It has
146 shown evidence of significant surface changes during the monitoring of the nucleus including motion
147 of decametre-scale boulders. The boundary with Atum sub-region a is clearly defined by the edge of
148 the rougher Atum material. The boundary with Atum sub-region b is also well defined by the small
149 cliff and the change in surface texture. However, there is also a change in texture between this sub-
150 region and the steep cliff that defines the Khonsu boundary with Bes. The sub-region is significantly
151 rougher in appearance. Figure 4 shows the roughness of the cliff leading up to Atum sub-regions b
152 and c. The right hand-side of the cliff is both higher and rougher. We define this as sub-region c and
153 it is indicated in brown in the 3D shape model maps.

154 A small smooth area can be distinguished between sub-regions a and b which we refer to as sub-
155 region e.

156

157

158



159

160 Figure 4 Left: OSIRIS image (NAC_2015-12-18T03.43.20) showing the Khonsu region and its relationship to Atum
 161 (particularly sub-region a) and Apis.

162

163

3. Ash (As) and Aten (An)

164

165

166

167

168

The Ash region on the body of the nucleus was defined as being an area covering much of the northern hemisphere and covered in a dust deposit that was assumed to be the result of sedimentation of non-escaping particles returning to the nucleus. The adjacent Babi region was not well observed during the first months of the mission. In particular, the surface towards Aker was ill-defined. The latest shape model has improved the definition of the interface to Aker markedly.

169

170

171

172

173

Ash is covered with dust but at $>6 \text{ km}^2$, it is the largest region in the nucleus definition. The small scale surface texture provides almost no assistance in defining sub-regions because of the dust coverage. Hence, we have used the shape model to look in detail at the topography and what can be seen of the substrate. In general, depressions have been isolated and cliffs or sharp changes in slope used to define boundaries. This has resulted in 10 different sub-regions (see also Figure 7).

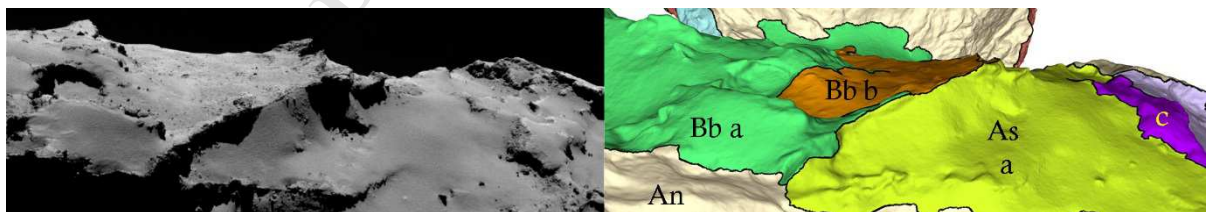
174

175

176

177

The interface to Babi is well defined by a topographic edge (Figure 5). Adjoining Babi at an edge and the Aten depression via a sharp change in slope, sub-region a adjoins an adjacent sub-region at a rough hummocky interface. The sub-region is mostly smooth with some smaller depressions and small cliffs covered in dust.



178

179

180

181

Figure 5 Left: OSIRIS image NAC_2014-12-02T07.59.13.739Z_ID10_1397549001_F23 showing the edge defining the interface between Ash and Babi. The shape model (right) shows sub-region a in yellow. The hummocky interface to sub-region c (purple) is also visible.

182

183

184

185

Sub-region b is bordered on one side by Seth (Figure 6). This sub-region is smooth. Its boundary to Seth is characterized by a transition to rougher terrain and a substantial change in slope. It is surrounded on two sides by sub-region c. The boundary with Seth is near the largest flat structure (Aswan) in that region.

186

187

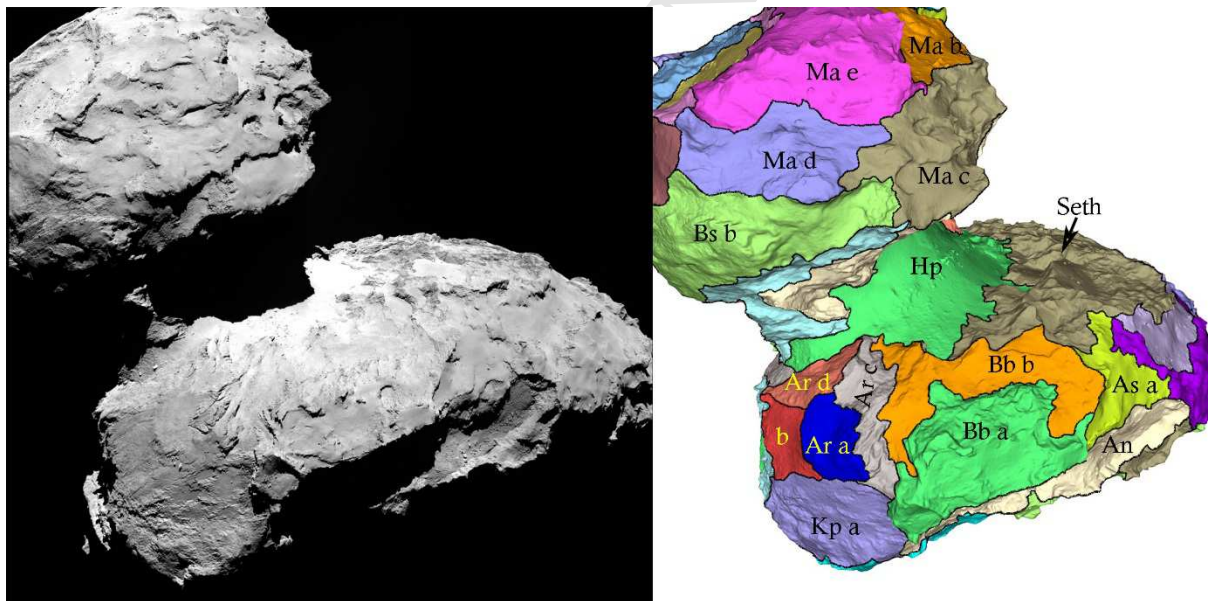
Adjoining Aten, sub-region c has rougher terrain. It is topographically higher than sub-region b and where it meets sub-region b there are arc-shaped cliffs. The cliffs are dust-covered.

188 Sub-region d is adjacent to sub-regions b and c. It is smooth and sits in a depression between a
 189 putative impact structure, the highly complex, very rough and extensive sub-region h, and the
 190 rougher terrain of sub-region b. The circular structure which is possibly of impact origin and what
 191 appears to be related material is defined as sub-region e (Figure 7). Sub-region d appear rather
 192 similar to sub-region b.

193 Sub-region f is mostly smooth with one significant irregular pit. It is bounded in the direction
 194 towards Atum by sub-region g. The boundary here is defined by cliffs. Sub-region g contains several
 195 quasi-circular depressions and is therefore similar to Seth which it bounds on one of its short sides.
 196 Sub-region g is topographically low compared to its surroundings but is bounded by a sharp change
 197 in slope at the interface to sub-region h.

198 Sub-region h is bounded by a planar surface with elevated topography (Apis) on one side and by
 199 the start of the Imhotep depression on another (Figure 8). The boundary to Ash sub-regions f and g
 200 is characterized by a sharp edge and a change in slope. The boundary to sub-region i is also
 201 characterized by an edge. Sub-region h has small scale roughness but limited larger scale roughness.

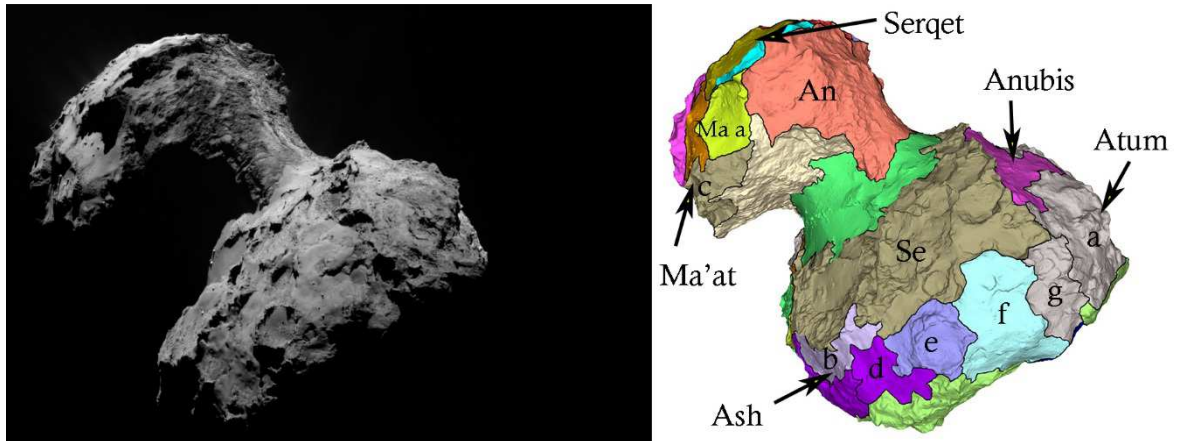
202 Sub-region i has major large-scale roughness with significant evidence of layering in cliffs. Sub-
 203 region j (Figure 9) borders Aten and is also a depression but not as deep as Aten. There is a ridge
 204 dividing two sections of the sub-region. The bases of the depression on both sides of the ridge are
 205 smooth.



206

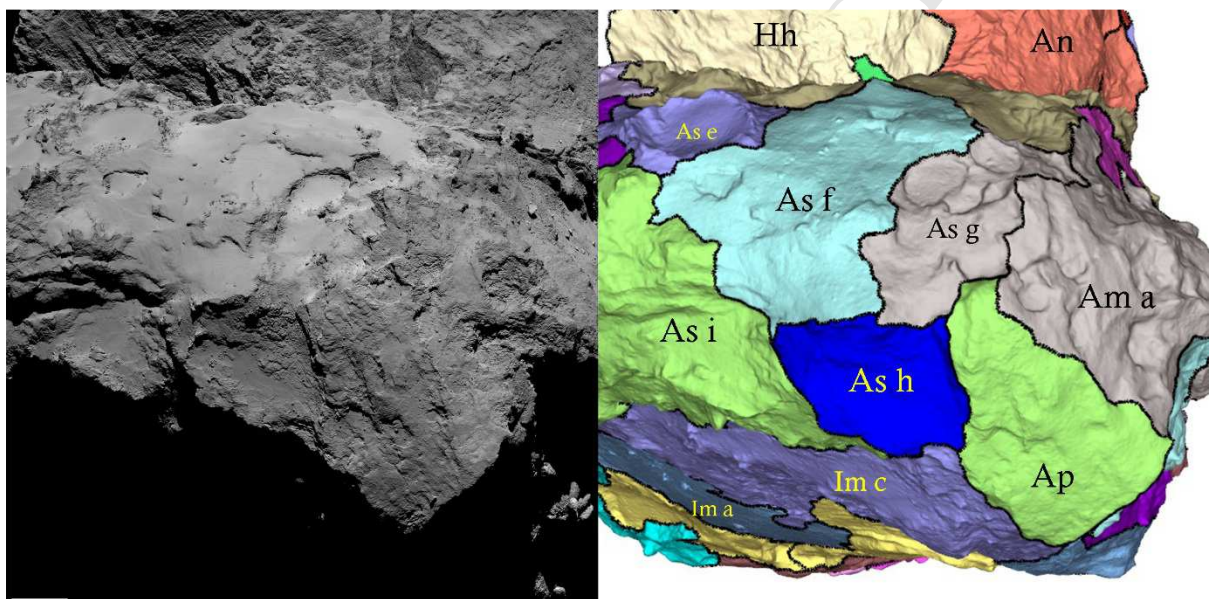
207 **Figure 6 Left: OSIRIS image NAC_2014-08-16T18.59.14. Right: The corresponding sub-region definition. Note the**
 208 **positions of the Aker sub-regions and their relationship to the two sub-regions of Babi. Note also the sub-regions of Ash.**

209 There appears to be little reason to sub-divide Aten. The depression structure and its interior are
 210 well-defined and there do not seem to be any significant changes or boundaries within it.
 211



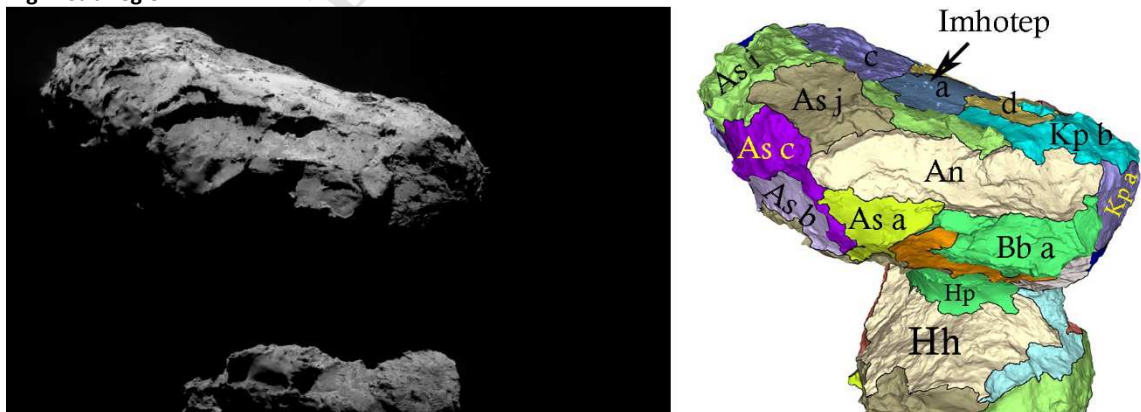
212
213
214
215

Figure 7 Left: OSIRIS image NAC_2015-05-11T20.29.18 Right: The sub-region definition. Note the circular structure defined as Ash sub-region e and the Seth-like part of Ash, sub-region g.



216
217
218
219

Figure 8 Left: OSIRIS image NAC_2014-09-02T12.44.22. Right: The sub-region definition. Apis and Atum show much reduced dust-coverage compared to Ash while the Ash sub-regions show different topography. Note the presence of layering in sub-region i.



220
221
222
223
224

Figure 9 Left: OSIRIS image NAC_2015-05-11T13.07.42. Right: The sub-region definition showing Aten at the centre of the body in this view. Note the brown coloured sub-region (Ash j) which is a dust-covered depression (but much shallower than Aten).

225

4. Aker (Ar), Babi (Bb), and Khepry (Kp)

226

227

228

229

230

231

232

233

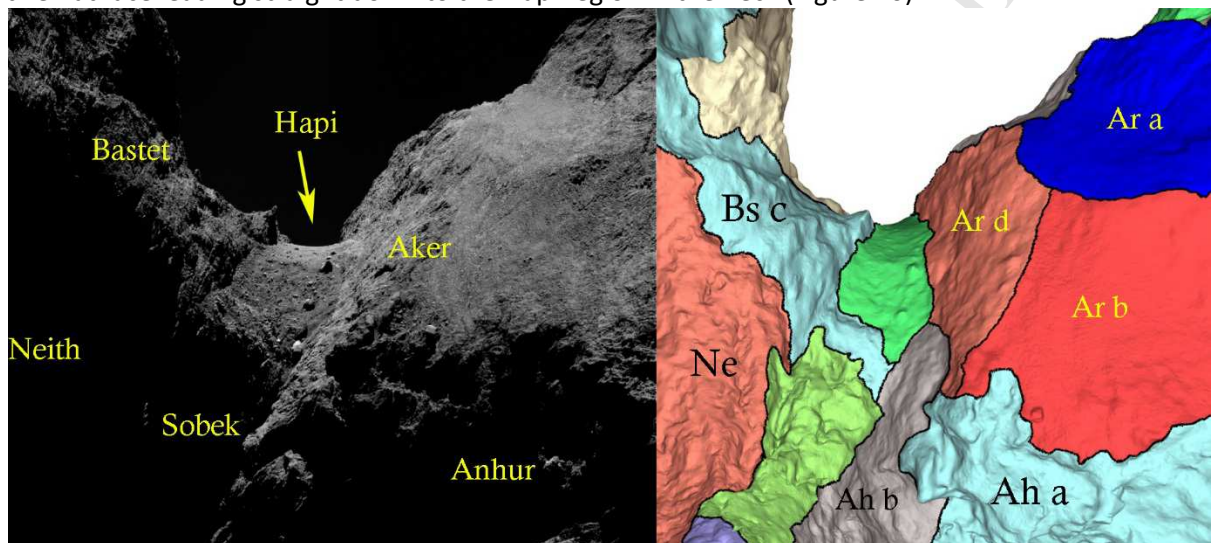
234

235

236

Aker is a highly unusual region (Figure 10). It has been split into four sub-regions reflecting four distinct faces of the surface in this region. Sub-regions a and b could be clearly seen in the early phase of the mission. Sub-region a is defined to contain the long (>200 m) tectonic fractures that were identified (Thomas et al., 2015). It is separated from sub-region b by a ridge. The boundary here is not extremely sharp but evident in images with low solar incidence. The basic appearance of the surfaces of these two sub-regions is very similar.

The early images gave poor coverage of the surfaces towards Hapi and towards Babi. Both are now shown to be steep cliffs associated with sharp changes in slope. They lead to Aker having an almost cube-like appearance. Sub-region c adjoins Babi and is characterized by a steep cliff with evidence of mass wasting (collapse). The face is not as regular as sub-region d. Sub-region d is a relative flat face leading straight down to the Hapi region in the neck (Figure 10).



237

238

239

240

241

242

243

244

245

246

247

248

249

250

251

252

253

254

Figure 10 Left: OSIRIS image NAC_2014-11-22T10.52.53.805Z_ID10_1397549000_F22. Right: The sub-region definition showing in particular the face of Aker leading down to the Hapi region in the neck.

Figure 6 also shows that Babi has been split in to two sub-regions characterized by very different large-scale surface roughness. The rougher sub-region, a, is dust covered on its northern facing surfaces but there are numerous quasi-circular structures and cliffs. The smoother sub-region, b, passes from the boundary with Ash below the cliffs to the interface (also a cliff) with Aker sub-region c. Most of the surface between Babi sub-region a and the Aker region is topographically low and has not been well-observed because it is surrounded on 3 sides by higher relief.

The Khepry region extends from Aker to Imhotep and is bounded by Babi and Aten on one side and Anhur on the other. The sub-region closest to Aker, sub-region a, is a flat but rock-like sub-region with ponded deposits. Sub-region c is topographically almost at right-angles to sub-region a and close to being in the same plane as most of the Imhotep region. It is a highly complex sub-region with rough, rocky terrain, smoother coatings in places and boulders. Talus from collapse of material from Ash is also evident. A small sub-region with a prominent cliff is defined as sub-region b. This adjoins Bes and is very similar to it. An alternative classification might assign this sub-region to the Bes region.

255

5. Imhotep (Im)

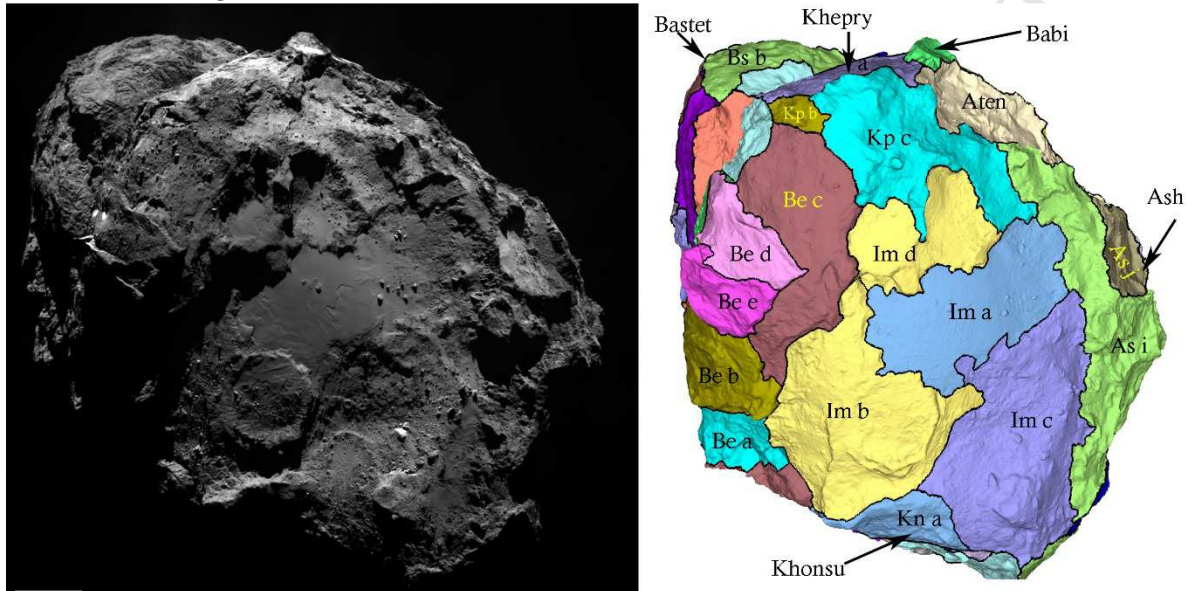
256

257

258

Imhotep is one of the most striking regions on 67P and was originally defined through being a large depression with its surroundings being at higher elevation. The texture of the surface in its interior is however remarkably diverse and we use this diversity to identify 4 sub-regions.

259 Sub-region a is the smooth terrain at the centre of Imhotep (Figure 11). It contains just a few
 260 boulders and shows surface features that changed throughout the mission. Sub-region b is at a
 261 notably higher elevation. It appears to be dust-covered in most places but is appreciably rougher in
 262 small-scale surface texture. It also encompasses a large, dust-filled, circular structure with layering.
 263 Sub-region c is rough on intermediate scales and contains the small circular structures that might be
 264 connected to similar features seen on Tempel 1. At the interface to sub-region a, there are layers
 265 that seem to have been exposed by some form of mass wasting and sub-region c, at its border with
 266 sub-region a, is at a significantly lower elevation. However, there are other structure within sub-
 267 region c that are at higher elevation.



268 **Figure 11** Left: OSIRIS image NAC_2015-04-29T17.24.09. Right: The sub-region definition for Imhotep.
 269
 270 Figure 12 shows an image taken from rotating the shape model to a specific orientation and
 271 illustrates the different surface types within Imhotep and the topographical relationships between
 272 them. The topographical changes between Imhotep, Ash and Apis are well seen in this view as well.



273 **Figure 12** View of the 3D shape model which emphasizes the topographic differences within the Imhotep region.
 274 The relationships of Imhotep (sub-regions a-c) to Ash and Apis are also well brought out in this view. The Bes sub-
 275 regions (a-e) are also evident on the left of the diagram. Two sub-regions (i and j) of Ash are marked.
 276

277

278

6. Anhur (Ah), Geb (Gb) and Bes (Be)

279

280

281

282

283

284

285

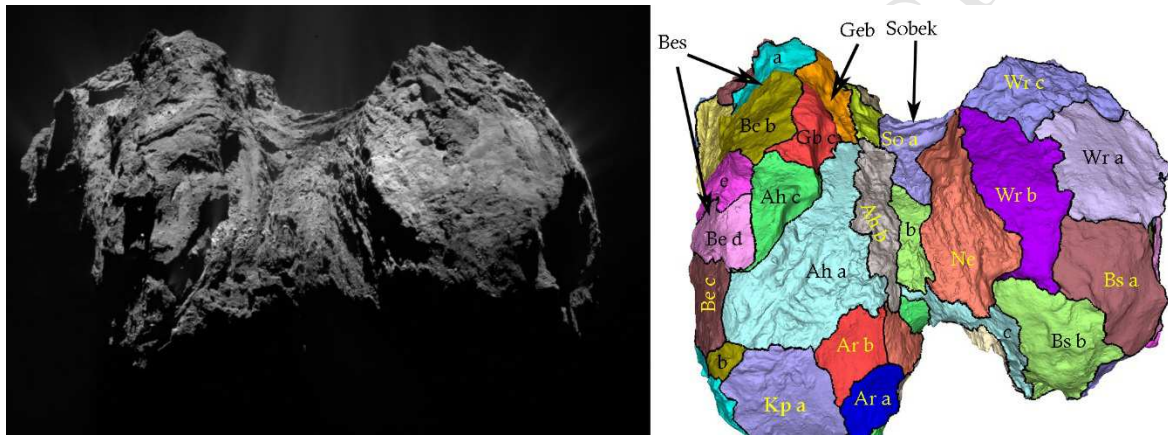
286

287

288

Anhur is of extreme intermediate-scale roughness and in the southern hemisphere. It bounds Aker and Khepy and extends down into the neck while being bounded elsewhere by Geb and Bes. The improved shape model shows that Anhur has three distinct parts (Figure 13). The intermediate roughness area adjacent to Aker and Khepy forms sub-region a. It is mostly a plateau with ridges and some pits. Sub-region b is almost orthogonal to it. The sub-region b cliffs are steep and form the transition from the body to the neck.

Sub-region c is similar to the Bes region. It contains a cliff and a plateau. The topographical relationship to Bes and Geb is also evident when the shape model is manipulated to a specific view (Figure 14).



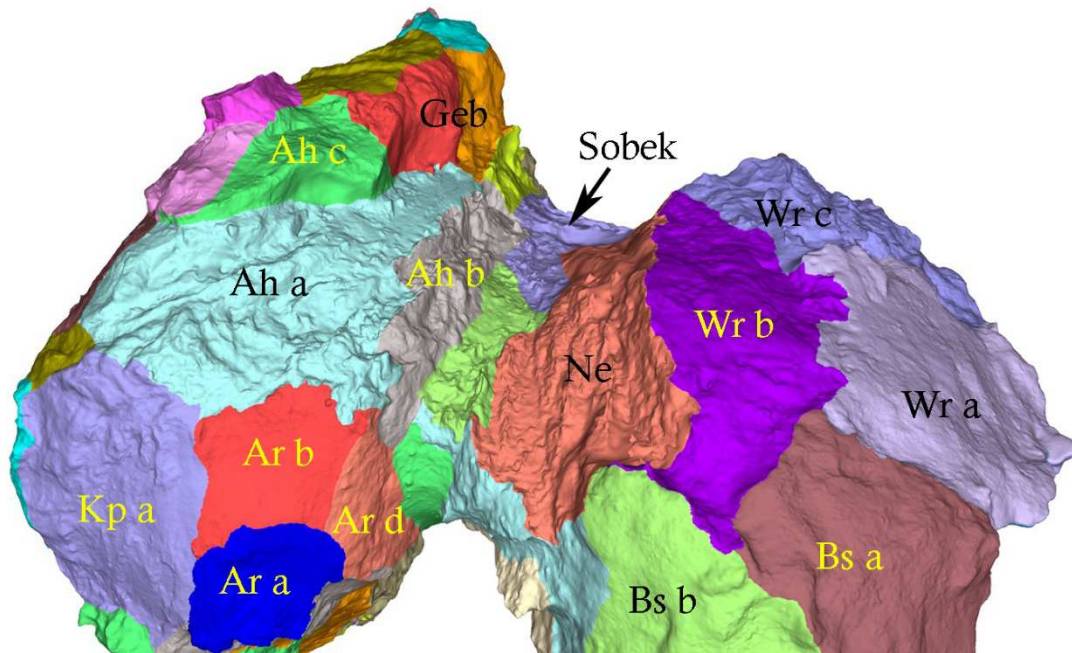
289

290

291

292

Figure 13 Left: OSIRIS image NAC_2015-08-01T13.51.57. Right: The sub-region definition. Anhur sub-region a (light blue) is bounded by the cliff (Anhur sub-region b) that descends into the neck. Note that Anhur sub-region c (green) has similar topographical properties to the Geb region



293

294

295

296

297

298

Figure 14 The shape model oriented to show clearly the topographic relationships between the different sub-regions of Anhur and the Geb region. The topographical relations within Wosret are also well-seen in this view. Other major sub-regions are marked.

The boundaries between Anhur sub-region c, Geb and Bes illustrate the importance of the shape model. The original southern hemisphere definition needed to be performed before the shape

299 model for the southern hemisphere was available. Having only a limited number of 2D images from
300 vertically above the area also reduced the topographic contrast and limited our understanding of the
301 topographic relationships. It is apparent here however that sub-region c of Anhur is most closely
302 related (structurally and textural) to Bes and Geb as previously pointed out by Fornasier et al. (2017).

303 Geb has been separated into 3 sub-regions. Sub-region b is similar to Anhur sub-region b. It is a
304 cliff dropping down to the bottom of the neck where it meets Sobek. The cliff is not quite as steep as
305 in Anhur and the surface is a little smoother. Sub-region c is the interface to Anhur sub-region c and
306 to the Bes region. It mostly comprises a steep cliff and the area close to its upper edge. The
307 boundary to Bes at this point is gradual and some uncertainty in the exact positioning is evident.

308 The most interesting element of Geb is sub-region a. This is also cliff-like but here the cliff is
309 highly fractured with numerous pits. Its surface appearance is most similar to areas in Wosret – on
310 the head of the nucleus (Figure 16) and distinguishes it clearly from other sub-regions in the vicinity.

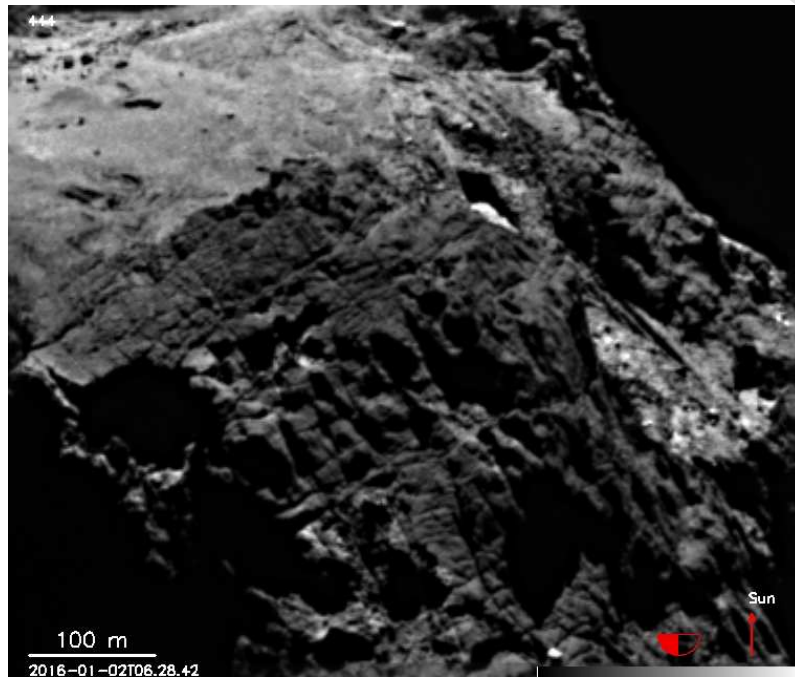
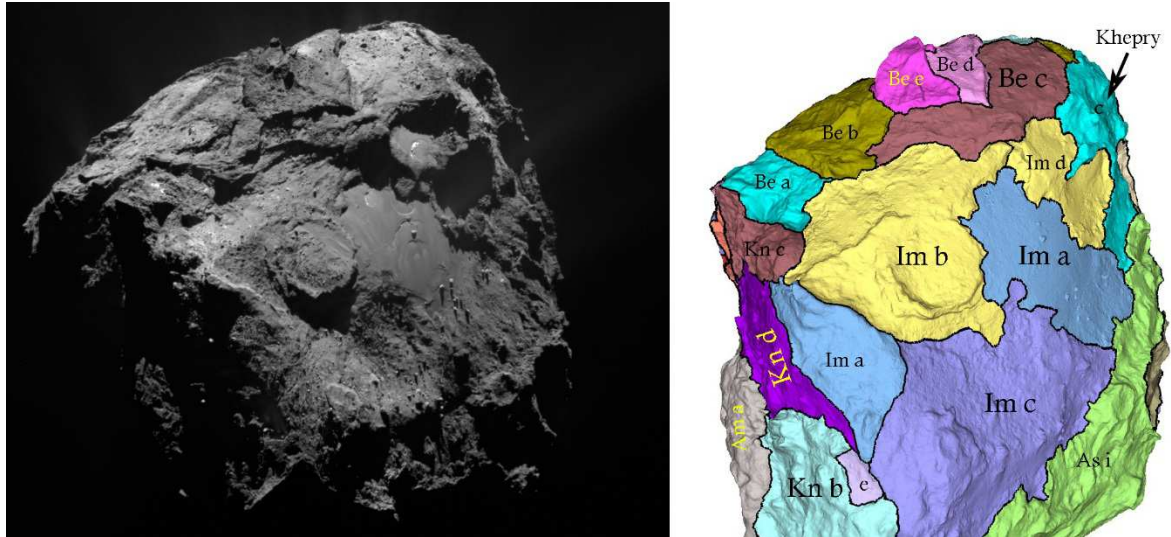


Figure 15 OSIRIS image acquired on 2 Jan 2016 at 06:28:42 showing sub-region a of Geb. The flat, smooth region above it is Anubis. The cliff of Geb is highly fractured and pitted.

311 Bes region has 5 sub-regions that are topographically distinct (Figure 16). This is most obvious
312 when the region is viewed obliquely from the direction of Khonsu and Atum. There are mostly
313 clearly defined step/cliffs leading from one topographic layer to another. The lowest level (sub-
314 region a) abuts Atum sub-region c and the Khonsu region. It is rough and strewn with boulders. One
315 side adjoins Imhotep. Here, the surface drops but not steeply into the Imhotep region. A cliff forms
316 the border with sub-region b of Bes.



317
318 **Figure 16** The Bes and Imhotep sub-region definition. Left: OSIRIS image NAC_2015-08-01T23.55.10. Right: The 3D
319 shape model. Bes mostly covers one long, thin face of the body of the nucleus with different topographical layers
320 delineated by steep cliffs.

321 The surface of sub-region b has boulders and a roughly diamond shaped set of ridges. Sub-region
322 c is reached via a small step downwards. Sub-region c is topographically higher than Imhotep (which
323 it abuts) and is separated from it by a cliff. Sub-region c is quite smooth at intermediate and large
324 scales.

325 A steep cliff separates sub-region d from sub-region c. It is at a higher topographic level and
326 probably higher than that of b. The top surface has boulders. Evidence of collapse of the cliff
327 material on sub-region c is present and blurs the exact definition of the base of the cliff. The
328 uppermost level is sub-region e. It is separated from d by a significant change in slope. The steep cliff
329 down to Anhur sub-region c is strongly apparent in the shape model.

330 The entire region gives the impression of distinct layers delineated by steep cliffs.

331 **7. Seth (Se) and Anubis (Ab)**

332 Seth and Anubis are both larger areas in the shape model. Seth, for example, covers 4.66 km².
333 However, the regional definition seems robust in both cases and there seems to be no requirement
334 to sub-divide these regions. The remarkable active pits (Vincent et al., 2016) and semi-circular
335 depressions (Ip et al., 2016) cover the entire Seth region. Anubis, on the other hand, has a very
336 smooth terrain. The boundary with Atum is gradual but the other sides are well-defined by
337 topography and the internal structure is smooth with some boulders. If further sub-division of
338 Anubis into units is performed in future, care must be taken with assessing surface changes as these
339 were significant in Anubis during the mission.

341 **ii. Neck**

342 **1. Hapi (Hp)**

343 The neck of the nucleus in the northern hemisphere is dominated by the smooth terrain mapped by
344 Thomas et al. (2015) and called Hapi. Here there is little reason to modify or sub-divide this region.
345 There are subtle exposures of more consolidated material in some places but these are very limited
346 in extent.

347

2. Sobek (So) and Neith (Ne)

348

349

350

351

352

353

354

355

356

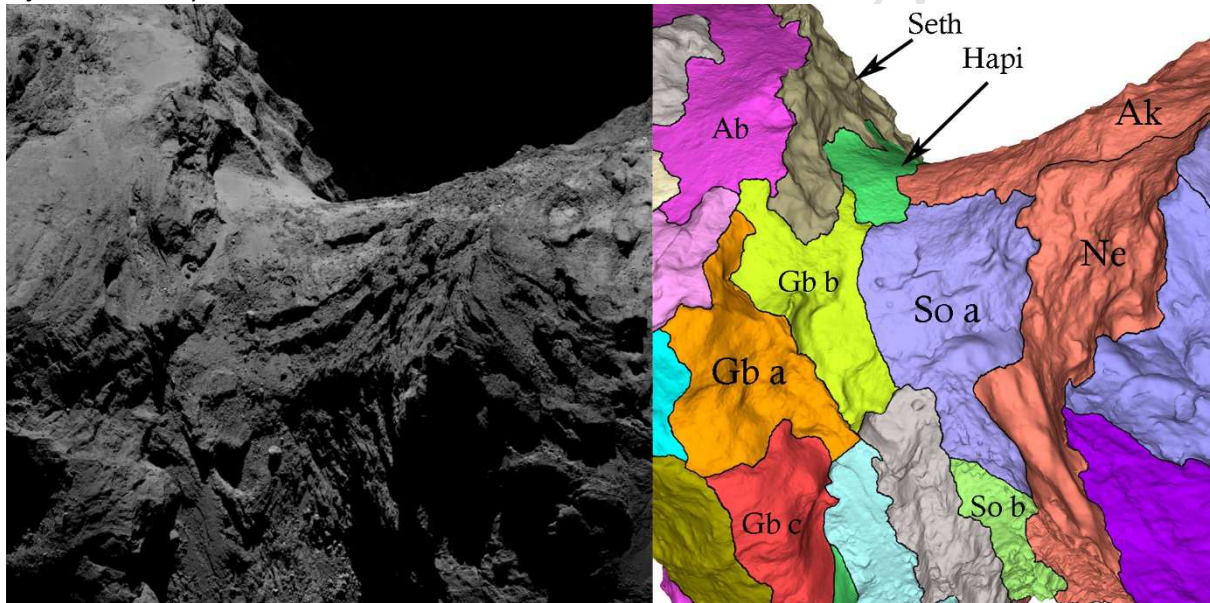
357

358

359

The neck in the southern hemisphere is considerably more complex texturally than in the north. Furthermore, there are some local areas where the shape model has a lower quality because of the absence of good quality images with adequate illumination. This particularly influences the Neith region. Neith is bounded by Wosret on one side and Sobek on the other. It forms the major steep cliff from an edge (the Neith-Wosret boundary) down into the neck itself. The surface is very rough on intermediate scales. There do not appear to be any large scale structures. Its surface appearance seems uniform. Hence, no sub-regions are proposed here.

Sobek is a long thin region running along the bottom of the “valley” between the head and the body. Its surface appearance is completely different to that of Hapi in the northern hemisphere. One end of Sobek (the Anuket end) is characterized by a series of steps (small cliffs) that are roughly orthogonal to the long axis of the neck (Figure 17). These steps have been observed to be a source of small jet-like activity.



360

361

362

363

364

365

366

367

368

Figure 17 Left: OSIRIS image NAC_2016-01-30T10.41.49.690Z_ID10_1397549900_F22. Right: The sub-region definition. The stepped structure of Sobek is evident at the centre of the image.

This stepped structure is confined to the Anuket end of Sobek and we define this as a sub-region (sub-region a). The transition to sub-region b comes from a small change in topography with sub-region b appearing to be at a slightly lower elevation. Across the boundary, the surface texture changes from larger small-scale roughness in sub-region a to a smoother terrain. However, sub-region b is not completely smooth and at the Hapi-Bastet end of the region there are a significant number of knobs and small cliffs – particularly at the interface to Neith.

369

iii. Head

370

1. Wosret (Wr)

371

372

373

374

375

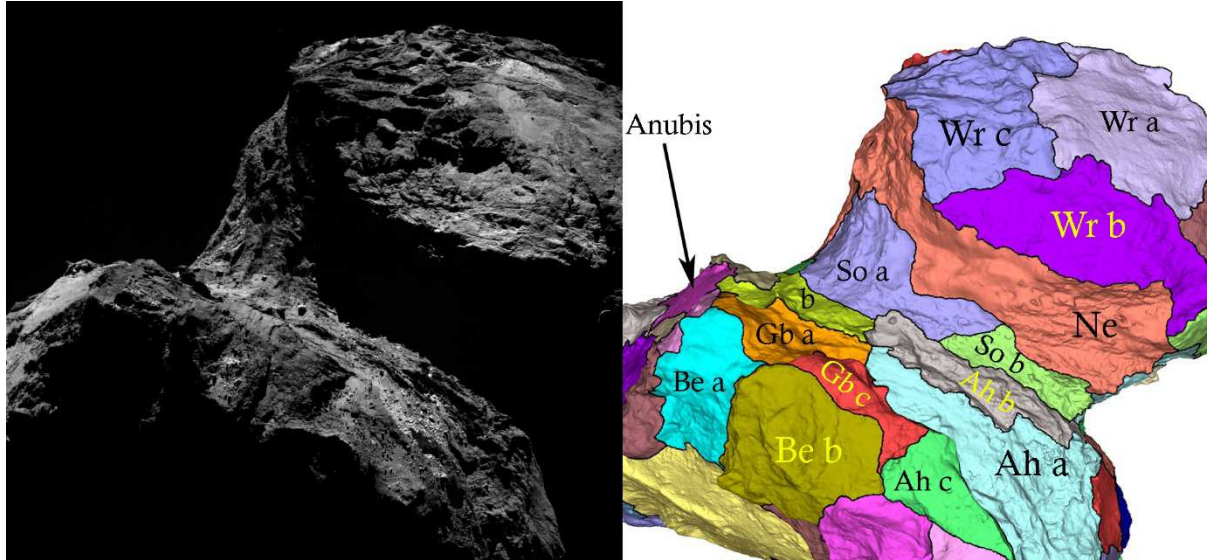
376

Wosret is a fascinating region. It gives the appearance of being a flat face on the southern side of the head of the nucleus. However, the shape model shows that this is not entirely accurate and the topographic and textural difference across the region can be clearly seen in suitable OSIRIS images (Figure 18).

Sub-region a is defined as a flat, smooth surface. It does contain a long, narrow intrusion that seems to have different reflectance properties but this has been ignored here. Sub-region b is

377 heavily fractured and it can be seen in Figure 18 that it is not planar with sub-region a. This is very
 378 evident in the shape model and the boundary has been defined along the line where the change in
 379 slope occurs. This line is not cliff-like but fairly straightforward to see in the shape model.

380 Sub-region c is defined according to the change in texture. This change is easily seen in Figure 18
 381 and comes from greater intermediate scale roughness. This roughness is evident as a combination of
 382 quasi-circular depressions (pits) combined with non-aligned ridges.
 383



384
 385 Figure 18 Left: OSIRIS image NAC_2016-01-02T17.23.24.646Z_ID10_1397549300_F22. Right: The sub-region
 386 definition. The Wosret region is particularly interesting in this image. The image shows the topographic and textural
 387 differences that have led to the definition of 3 sub-regions.

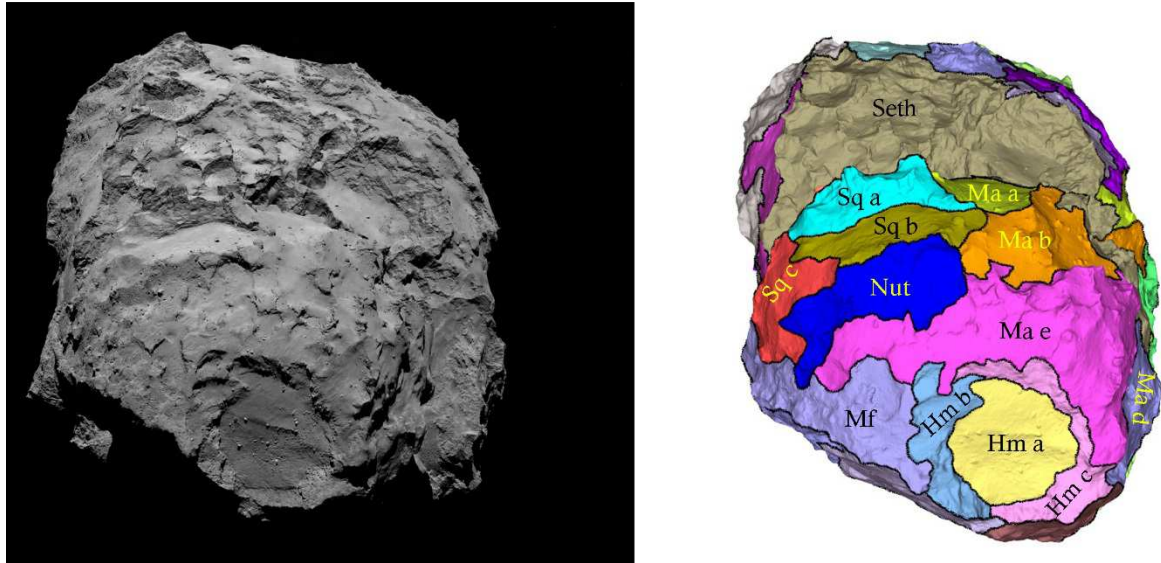
388 2. Hatmehit (Hm)

389 Hatmehit was one of the places on the nucleus to give a clear impression of being a single unit
 390 when the spacecraft arrived at the comet. The circular appearance of the whole structure is very
 391 striking. However, in detail, the structure is not symmetric and we split the structure into 3 sub-
 392 regions to reflect this (Figure 19).

393 Sub-region a is the smooth almost circular surface area in the centre of the region. This
 394 straightforward definition has an advantage in that, while it is widely assumed that the Hatmehit
 395 interior has been produced by the same process that produced the rim, a relationship has not
 396 actually been proven. Production via an impact phenomenon of some sort might be a hypothesis but
 397 it must explain the flat nature of the interior and the differences between the two sides of the rim.

398 Sub-region a has a small change in slope passing through its centre. However, there seems to be
 399 no other textural change associated with this. The presence of talus and dust cover prevents any
 400 further sub-division.

401 Sub-region b abuts Wosret and Maftet. This sub-region shows a transition to the Maftet-like
 402 surface. The gain in elevation from sub-region a to the Maftet boundary is gradual. Within this, there
 403 are arcuate depressions. In sub-region c, on the other hand, the transition to Bastet and Maat is
 404 much steeper. The surface is rock-like and heavily fractured in places. There are steep cliffs that are
 405 arcuate near the interface with Maat and some evidence of layering (Giacomini et al., 2016).
 406



407
408
409

Figure 19 Left: OSIRIS image NAC_2014-08-06T01.19.14. Right: The sub-region definition showing the nucleus along its long access with Hatmehit in the foreground.

410

3. Serqet (Sq) and Nut (Nu)

411

Serqet is a remarkable region and we have sub-divided it into 3 sub-regions. The most remarkable aspect is that the surface changes from a smooth, dust covered, horizontal plane to an almost vertical rock-like structure at a very distinct boundary. The sub-region definition separates these two areas (Figure 20).

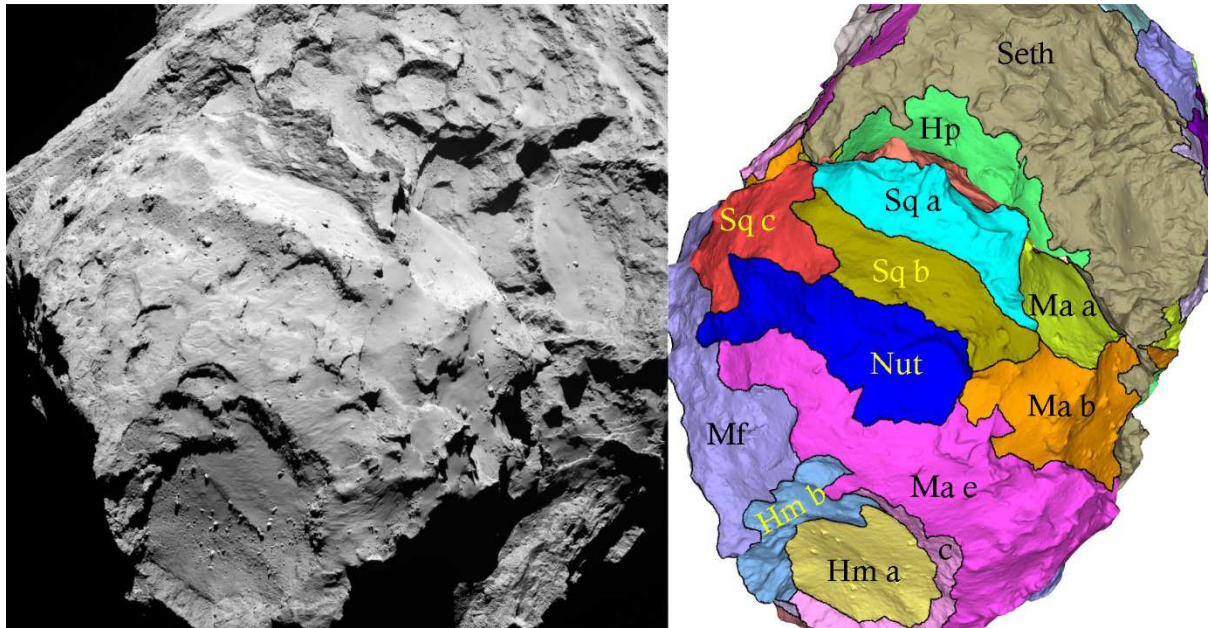
415

In the original regional definition, Serqet was extended to meet Maftet. The coverage of this area at the time was rather poor. The shape model shows there is a rapid change of slope between sub-regions a and b and the rest of Serqet. Hence, we define this transitional surface as being sub-region c. This evidence for some quasi-circular and arcuate depressions in sub-region c suggests that the substrate has some similarity to the adjacent Maftet region.

420

The shape model confirms the impression given in the first data that Nut is a depression distinct from Serqet and the Maat region on its opposite side. The shape model shows that the change in slope at the boundary to Serqet sub-region b is similar to that seen at the sub-region a to b boundary although 2D images alone completely fail to give this impression. There does not seem to be any justifiable reason to sub-divide Nut.

424



425
426
427
428

Figure 20 Left: OSIRIS image NAC_2015-03-05T00.38.41.069Z_ID10_1397549003_F41. Right: The sub-region definition showing Serqet in the centre of the image. Ma'at sub-regions a and b are also evident to the right of Serqet. The Hatmehit sub-regions (a, b, and c) are also marked.

429

4. Ma'at (Ma)

430

Like Ash on the body of the nucleus, Ma'at was defined through the dust coverage on north-facing surfaces. We take the same approach with Ma'at as taken with Ash and look at topographic differences and evidence of non-uniformity in the substrate to define sub-regions. The process has resulted in 5 distinct sub-regions (Figure 21).

434

Sub-region a is a smooth, shallow depression with numerous knobs. It adjoins Anuket and Serqet. A ridge separates sub-region a from sub-region b which also adjoins Serqet. The surface of b is similar but contains an irregular structure close to its centre. In this region, there are numerous knobs visible that are probably the topographic expressions of the substrate through the dust covering.

439

Sub-region c contains a number of quasi-circular pits that have been shown to be active. There are several arcuate depressions superposed on a substrate that seems to have significant large scale roughness. Its topographic appearance is similar to parts of Seth and one of the Ash sub-regions.

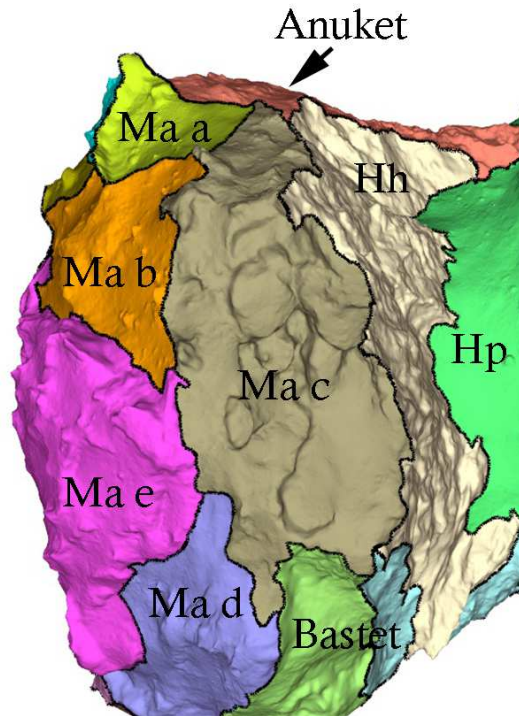
442

Sub-region d is a plateau and more planar than the rest of the region. It is bounded by an abrupt, sharp change in slope at its boundary with Bastet. The boundary with sub-region e is a cliff of intermediate slope. A knobby ridge is present near its centre.

445

Sub-region e covers the rest of Maat. It is dust-covered but the substrate is obviously rough on large scales. It becomes smoother towards the boundary with Nut but this is gradual.

446



447
448 **Figure 21** The shape model showing the 5 sub-regions of Maat. Note the different surface appearances.

449 **5. Bastet (Bs)**

450 The boundaries between Bastet, Hathor and Wasret were poorly observed during the early
451 phase of the mission and good observations were only obtained as the comet reached equinox
452 inbound.

453 A single really good view of the Bastet region is not straightforward because the region has been
454 defined as going from the Wasret (south-facing) region to the Hathor region on the opposite of the
455 head. The region appears to have 3 components. The sub-region adjoining Wasret is undulating but
456 with small scale roughness and little or no deposited dust. The border with Wasret is mostly defined
457 through a small scarp.

458 Sub-region b is defined at a sharp change in the surface plane as the region wraps around the
459 head. This sub-region has a U-shaped depression and has more large-scale roughness than sub-
460 region a.

461 Sub-region c has significant intermediate scale roughness and is possibly a transition region
462 between the smoother terrains of sub-regions a and b and the fractured, rocky appearance
463 associated with the ~900 m high cliff dominated, Hathor. Sub-region c is not planar with Hathor. Its
464 extent down into the neck is not easily determined. In this part of the sub-region, there is similarity
465 in surface appearance to both the Neith region and part of Sobek sub-region b. This leads to some
466 ambiguity.

467 **6. Anuket (Ak), Hathor (Hh) and Maftet (Mf)**

468 The improvements in the shape model do not suggest the need for sub-division of these regions.
469 Hathor is dominated by the 900 m high cliff that drops from the Ma'at region on the head to the
470 Hapi region in the neck. The roughness and the appearance of the cliff may not be perfectly uniform
471 across its surface but there are certainly no obvious differences that would suggest a major
472 advantage in sub-dividing the region.

473 Similarly Anuket is fairly uniform in appearance being mostly smooth at intermediate and large
474 scales but with small scale roughness giving a rocky appearance. The boundary with Neith is gradual
475 but the boundaries with Serqet, Hathor and Hapi are extremely clear.

476 Maftet is dominated by quasi-circular and elliptical depressions with a significant dust covering.
477 There are gradual transitions towards Hatmehit and Serqet but there do not appear to be any
478 intermediate scale differences in the surface properties (either structurally or topographically) to
479 require sub-division.

480 **3. Derived products**

481 **a. Surface areas**

482 The total surface area of the nucleus with this model is 51.74 km² (Preusker et al., 2017). The
483 derived surface regions and sub-regions can be used to determine some values of interest. It should
484 be noted that we use the following only as examples of the way in which the surface areas derived
485 here might be used.

486 **i. Airfall deposits**

487 Ma'at, Ash, and Babi are regions that are mostly dust-covered probably as a result of
488 transport/sedimentation of dust (Thomas et al., 2015). They are pre-dominantly in the northern
489 hemisphere. The dust covering is associated with non-escaping particles emitted from the Hapi
490 region and the southern hemisphere (Thomas et al. 2015; Keller et al., 2017). The total area of the
491 three regions is 11.53 km² or 22.3% of the total surface. There are sub-regions that appear less
492 covered or devoid of these deposits. Excluding these from the calculation gives 9.43 km² (18.2%).
493 Seth has several north-facing probably dust-covered surfaces but these would have to be included
494 individually in any calculation as there are numerous vertical surfaces within the region that
495 contribute to the total area. We note that some authors may choose to assume that the surfaces of
496 parts of Imhotep, Serqet, Maftet, and Anubis are also influenced by sedimenting dust.

497 **ii. Smooth (changing) surfaces**

498 The regions of Anubis, Hapi and parts of Imhotep (sub-regions a and d) are smooth and inferred
499 to be dust covered. They also exhibit surface changes that are inferred to be related to activity (El-
500 Maarry et al., 2016) following the appearance of quasi-elliptical depressions. The surface area of
501 these regions and sub-regions is 4.49 km² (8.7%). Serqet sub-region b also appears to be dust-
502 covered and smooth. However, no evidence for quasi-elliptical depressions has yet been presented
503 for Serqet.

504 **iii. Fractured cliffs on the head**

505 The head of the nucleus has three main regions that are almost orthogonal to local gravity and
506 comprise fractured or rough terrain leading down into the base of the neck. These regions are Neith,
507 Hathor, and part of Bastet (sub-region c). These regions comprise 8.3% of the surface area of the
508 nucleus. Anuket is the only other region which drops to the neck on the head side of the nucleus.
509 However, the surface of Anuket, which has a surface area = 4.0% of the whole nucleus, is more
510 consolidated.

511 **iv. Regions with pits**

512 The presence of active pits on the nucleus was one of the more remarkable results from the
513 observations of the nucleus. Activity was observed from pits in the Seth and Ma'at regions (Vincent
514 et al., 2015) specifically. In Ma'at, the pitted structures are restricted to sub-region c in our
515 definition. Furthermore, structures looking very similar to those seen in Seth are apparent in Ash
516 sub-region g (see also Ip et al., 2016). These three sub-regions alone contribute 11.6% of the surface
517 area (although $\frac{3}{4}$ of that area is solely Seth's contribution). Some parts of Atum also show some
518 quasi-circular structures that might be related and isolated pits are evident elsewhere. Fornasier et
519 al. (2017) noted the presence of an active pit in Anhur. Hence, around 11-15% of the surface area
520 shows evidence of larger scale pits that are either active during the present perihelion passage or (by
521 analogy) were active in the past.

522 **v. Arcuate surfaces**

523 Maftet shows a large number of arcuate depressions that are generally shallow compared to the
524 pits seen in Seth or Ma'at. These structures are also seen in the rim of Hatmehit (sub-region b) and
525 gradually disappear as one crosses the Serqet c transitional region. Including the whole of Serqet c,
526 this results in a contribution to the surface area of 2.6%.

527 **vi. The Bes plateaux**

528 The shape model shows the sub-regions b, d, and e of the Bes region having distinct scarps and
529 suggest some form of large scale layering. The corresponding surface areas are 0.65 km^2 , 0.32 km^2 ,
530 and 0.34 km^2 respectively. The cliffs have been seen to be active and hence a volume estimate may
531 provide some insight into the available volume of source material. The plateaux sit topographically
532 on top of Bes sub-region c on the equatorial side of the nucleus and the material exposed as the
533 steep cliffs of Geb (sub-regions a and c) and Anhur (sub-region c). Although these cliffs seem very
534 prominent in the 3D shape model, the total surface area of these 3 sub-regions only covers 1.9% of
535 the nucleus.

536 **b. Morphological roughness**

537 **i. Regional**

538 The definition of the roughness of a non-planar (3D) surface is not trivial. Issues include the scale
539 length over which the roughness is computed and whether the large-scale curvature of the body is
540 removed and how that is actually performed. This problem is one encountered in the computer
541 graphics industry. For this work, we look at the relative roughness between regions using a
542 technique developed by Lavoué (2009) for this purpose. The reader is referred to Lavoué (2009) for
543 details but we give a brief summary of the key points of the algorithm.

544 In this algorithm, for each vertex of the shape model, the curvature tensor is calculated and then
545 the principal curvature values (k_{\min} , k_{\max}) are extracted. These correspond to the eigenvalues of the
546 curvature tensor. For the roughness estimation algorithm, the maximum curvature k_{\max} , is
547 determined since this value reflects the bumpiness of the surface.

548 The roughness measure of Lavoué is then based on a scale parameter which determines the
549 frequencies that have to be considered as roughness. In order to establish this scale parameter, a
550 local window of a mesh is defined. Although the concept of a local window is trivial in 2D image, it
551 becomes significantly more complex for 3D objects on an irregular mesh. Lavoué defines the local

552 window of a single vertex by using a sphere of definable radius and determining where this sphere
 553 intersects with the mesh. The algorithm is then based on the average curvature difference between
 554 the original object and a smoothed version where the smoothing distance is linked to a scale
 555 parameter that is in turn linked to the radius of the local window. It is this step that allows
 556 determination of roughness over different scale lengths. It also eliminates resolution issues in
 557 studying facet-to-facet roughness. Facet-to-facet roughness suffers from resolution issues and the
 558 noise in the facet determination algorithm.

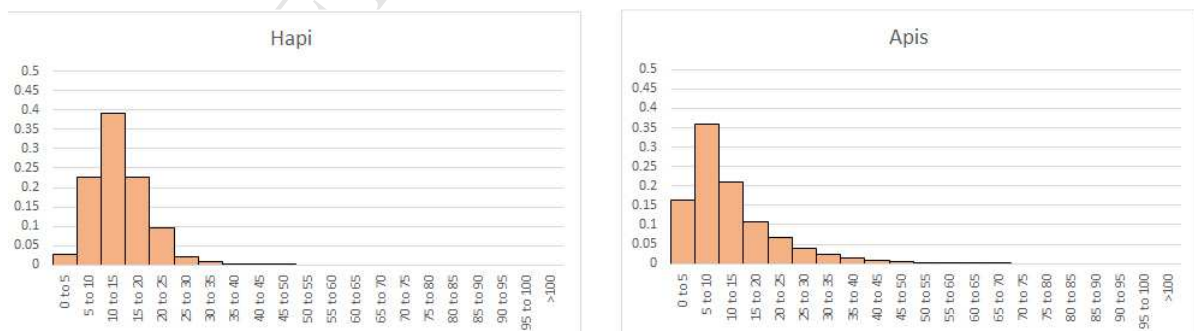
559 The approach is quantitative in the sense that a numerical value for the roughness can be
 560 extracted. However, the interpretation of the numerical result in terms of a slope distribution is not
 561 straightforward because the algorithm is effectively determining average curvature differences
 562 between the original object and a smoothed version of that object on a scale length given by the
 563 scale parameter. Hence, the algorithm is adequate for comparisons between regions on 67P and
 564 allows us to make statements about relative roughness differences with some level of confidence.

565 It should be noted that in the published algorithm, the scale of the roughness is expressed as
 566 percentage with respect to the size of a bounding box that surrounds the surface being investigated.
 567 This implies that regions that have different total sizes would be examined for roughness over
 568 different scale lengths. With the help of the author (Lavoué, pers. comm.), we have implemented a
 569 small modification so that roughness is characterized over a fixed distance irrespective of the total
 570 size of the region. We have used here 20 metres as the roughness scale which is around 20 times
 571 larger than the quality of the SHAP7 model.

572 In Figure 22, we show a plot of histograms of the roughness values for the Apis and Hapi regions.
 573 Both these regions are relatively flat and smooth over large areas and distances. The surface of Apis
 574 does not appear dust covered. The y-axis of the plot shows the areas of facets in each bin
 575 normalized to the total area of all facets in the region. The x-axis gives the bins and is given in
 576 curvature units, [1/km]. This follows the definition of Cauchy who defined the centre of curvature as
 577 the intersection point of two infinitely close normals to a curve, the radius of curvature as the
 578 distance from the point to the centre of curvature, and the curvature itself as the inverse of the
 579 radius of curvature thereby giving the expressed units. Clearly, the larger the value, the greater the
 580 roughness through lower radii of curvature.

581 The shape of the curve resembles a Maxwell-Boltzmann speed distribution but this is a
 582 coincidence and attempts to use this type of mathematical distribution as a fitting formula produce
 583 nonsensical results. Hence, we have merely fit the peak with a Gaussian and express the results as
 584 the position and width of that Gaussian in order to give two easily interpretable numerical values
 585 describing the distribution.

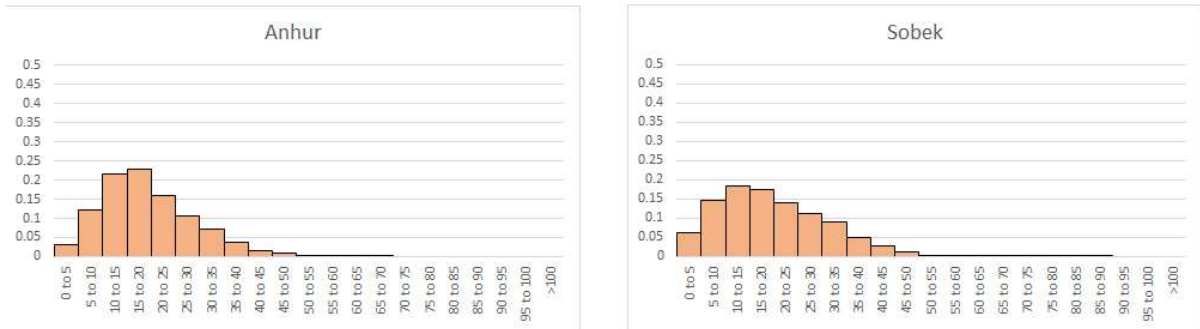
586



587
 588
 589
 590

Figure 22 A quantitative expression of the roughness of the Apis and Hapi regions on the nucleus. The y-axis expresses the normalized area in each bin. The x axis defines the effective curvature difference between the original object and a smoothed version of that object with a scale parameter equal to 20 m.

591 Figure 22 should be compared to Figure 23 which shows the same plot but for the Anhur and
 592 Sobek regions. The histograms are markedly different from the Apis and Hapi results. This indicates a
 593 quantitative difference in roughness between the Anhur-Sobek regions and the Apis-Hapi regions
 594 that agrees with their subjective appearance.



595
596
597

Figure 23 As Figure 22 but for the Anhur and Sobek regions. Notice that the distribution is much broader indicating a large distribution of roughness. The peak of the distribution is also shifted to higher roughness values.

598
599
600
601
602
603
604
605
606

In Table 2, we take this a step further by computing the peak and the width ($1/e$ width) of the distributions for each region. As stated above, a Gaussian fit has been used here to identify the peak although there is no doubt that the exact functional form of the distribution is significantly different from a Maxwellian. Nonetheless, we are simply trying to identify if the roughness measure gives numerical support to our subjective impression that some areas are rougher than others. It should be noted that the tail of the distribution influences the position of the Gaussian peak and so distributions with a long tail will produce positions of the maxima that are at higher values than the maximum probability. Through modifying the box size, we estimate the “error” in the values to be of the order of ± 2 although this is a somewhat subjective value.

607
608
609
610
611

The results in Table 2 are quite informative. For example, it is confirmed that regions such as Khonsu, Atum, Sobek, and Hathor are indeed very rough with Sobek being quantitatively the roughest of these four. Anhur is rougher still. Bes is also rough despite the fact that its plateaux are well organized and layer-like. This might indicate an issue with the method where regions are defined with respect to layers with steep slopes.

612
613
614
615
616
617

The smoother regions include (apart from Hapi and Apis) Aker and Anubis as one might expect. Babi is, perhaps surprisingly, smooth in the peak roughness metric. However, it is noticeable that the width of the distribution for Babi is considerably broader than for the other smooth terrains. This may reflect the fact that Babi has two distinctly different types of terrain that we have separated into two sub-regions. Although both sub-regions are dust covered, Babi a has significant large scale roughness while Babi b is much smoother.

618
619
620
621
622
623
624
625
626
627

Both Anuket and Imhotep give the visual impression that they are fairly smooth but, in both cases, the roughness parameter suggests these surfaces are rougher than, for example, Maftet or Bastet, respectively. In the case of Anuket, the surface is rather uniform in visual appearance and this is substantiated by the lower value for the width of the distribution when compared to regions with a similar peak roughness parameter. Imhotep is far more diverse in surface morphology which has resulted in our defining 4 sub-regions. However, the width of the distribution is actually less than the value for Anuket. This leads to the conclusion that while these statistics are broadly following our perception and giving numerical confidence to our interpretation of surface roughness differences, blindly accepting the numerical results might lead to misinterpretation in certain specific cases.

628
629

Table 2 The roughness parameters for each region giving the peak bin and the width of the distribution.

Region	Peak roughness parameter	Width of roughness distributions
Hapi	8.36	5.31
Anubis	11.63	4.36
Geb	12.27	6.9
Babi	12.6	11.91
Apis	12.77	5.03

Ma'at	12.99	10.43
Hatmehit	13.79	7.45
Aker	14.1	6.44
Serqet	14.13	7.69
Nut	14.33	6.72
Bastet	14.76	7.27
Imhotep	15.14	7.22
Khepry	15.71	6.89
Ash	15.74	9.45
Seth	16.16	12.65
Aten	16.75	12.1
Maftet	16.92	8.61
Anuket	17.01	7.83
Atum	17.09	8.69
Bes	17.15	8.17
Wosret	18.26	8.59
Neith	18.63	15.1
Khonsu	18.83	8.46
Hathor	19.6	8.66
Sobek	21.4	9.85
Anhur	24.47	13.96

630

631

ii. Sub-regional

632

The computation of the roughness parameters has also been made for the 71 sub-regions identified in Table 1 and we look at some specific examples.

633

634

635

636

637

638

639

640

641

642

643

644

Imhotep has four sub-regions with sub-region a being very smooth and a site where surface changes were observed. In Table 3, we show the peak of the roughness distribution function for the four individual sub-regions of Imhotep and sub-regions of note elsewhere. As expected, the smoothest sub-region of Imhotep has the lowest roughness parameter with a value of below 10 and only slightly higher than that of Hapi. Sub-region d, which also showed evidence of changes and dust coverage is shown to be rougher (presumably arising from the depression rims surrounding the dust deposit) while sub-regions b and, particularly, c are indicated as being much rougher although not as rough as Sobek, Anhur (sub-regions a and b), or Neith. This result confirms quantitatively the visual perception.

Table 3 Peak roughness parameter for the individual sub-regions within some regions

Region	Sub-region	Peak roughness parameter
Imhotep	a	9.58
	b	16.7
	c	17.52
	d	12.78
Hatmehit	a	10.36
	b	16.14
	c	17.91
Serqet	a	18.8
	b	11.96
	c	13.7

Babi	a	16.61
	b	9.59
Anhur	a	27.06
	b	25.53
	c	7.28

645

646

647

648

649

Hatmehit shows a similar result. The central dusty sub-region (sub-region a) has a roughness parameter comparable to but slightly higher than that of Imhotep sub-region a. The rim of the “crater” is appreciably rougher with the arcuate sub-region (b) being slightly less rough than the cliff-like sub-region.

650

651

Serqet has a cliff (sub-region a) and a dusty, relatively smooth sub-region at the base of the cliff (sub-region b). Table 3 again indicates quantitative agreement with the perception.

652

653

654

655

656

657

Babi was referred to above as having a broad distribution and indeed the two sub-regions that have been defined have very different roughness parameters. Sub-region b has a value of 9.59 (a value seen for smooth sub-regions) while the value for sub-region a is 16.61 placing this sub-region at a roughness level similar to rougher areas of Ash. Here again, the perception of significant variation within the region is confirmed and a difference between the defined sub-regions is apparent.

658

659

660

For Wosret, the very rough pitted terrain of sub-region c is also identified in the analysis as being very rough (24.49) with the flatter face (sub-region a) being clearly smoother (13.58). The fractured terrain towards the neck is intermediate.

661

662

663

664

665

666

667

668

The roughest sub-region is Sobek sub-region b (31.78) while the smoothest is (perhaps surprisingly) Geb sub-region c (6.90). The latter forms part of the steep cliff leading up to the Bes region and is completely devoid of boulders. The width of the distribution is however quite large (10.41). By comparison, the Imhotep smooth sub-region (sub-region a) has a distribution width of only 3.30 indicating greater uniformity as is apparent in the images. It is to be noted that Anhur sub-region c, which adjoins Geb sub-region c has a similar low value of the roughness parameter (7.28 and the second lowest value of all sub-regions). This suggests that Anhur sub-region c might have been better defined as part of Geb.

669

4. Summary and Conclusions

670

671

672

673

674

675

676

677

678

679

680

681

682

683

The definitions of regions on the nucleus that were originally made on 2D images (Thomas et al., 2015; El-Maarry et al. 2016;2017) can be mapped back onto the shape model of the nucleus (SHAP7; Preusker et al., 2017) to provide a self-consistent definition in three dimensions. The accuracy of the SHAP7 model (metre-scale) and the use of 3D tools have allowed us to ensure that the regional definition is complete. Detailed study of the shape model in combination with 2D images indicates that many regions can be further sub-divided into sub-regions of common morphology. This is particularly true in regions that had been only poorly imaged at the time of the original regional definition – notably the neck of the nucleus in the southern hemisphere. We provide a comprehensive table of these sub-regions and have mapped them onto the 3D shape model. Detailed comparisons between the sub-region definitions and 2D images acquired by OSIRIS have been presented to justify our interpretation and definition.

We have illustrated the use of the surface areas to compute the total surface areas of morphological types on the nucleus..

684

685

686

687

688

We have used the SHAP7 model and the regional definition to compute a quantitative measure of surface roughness for each region. The algorithm has been proposed for computer graphics applications (Lavoué, 2009) and gives a measure for the roughness that broadly agrees with our perception of the roughness from visual (2D) images and the appearance of the shape model. The algorithm identifies Sobek and Anhur as the roughest regions on the nucleus while Hapi

689 (unsurprisingly) and the flat-faced rocky surface of Apis are the least rough on regional scales. When
690 running the algorithm on the sub-region definition, results consistent with our separation of
691 different terrain types into sub-regions can be found. In particular, the sub-region definitions of
692 Imhotep, Babi and Wosret appear to be well justified. While this algorithm has some drawbacks,
693 particularly the absence of a clear physical relationship to the derived parameters, the relative
694 ordering of regions and sub-regions with respect to their roughness parameters appears to have
695 potential for helping define surface units with common properties.
696

697 ***Supplementary material***

698

699 To support use of these regional definitions, we provide a VTK file linking the facets directly to
700 the regions for the 12 million facet SHAP7 model. We have chosen VTK format because the facets
701 and the region definition are contained within one file and the need to correlate after importing of
702 two files into a software is avoided. VTK files can be imported into 3D visualization tools such as
703 ParaView™.
704

705 **Acknowledgements**

706

707 The team from the University of Bern is supported through the Swiss National Science Foundation
708 and through the NCCR PlanetS. The project has also received funding from the European Union's
709 Horizon 2020 research and innovation programme under grant agreement No 686709. This work
710 was supported by the Swiss State Secretariat for Education, Research and Innovation (SERI) under
711 contract number 16.0008-2. The opinions expressed and arguments employed herein do not
712 necessarily reflect the official views of the Swiss Government.
713

714 OSIRIS was built by a consortium led by the Max-Planck-Institut für Sonnensystemforschung,
715 Göttingen, Germany, in collaboration with CISAS, University of Padova, Italy, the Laboratoire
716 d'Astrophysique de Marseille, France, the Instituto de Astrofísica de Andalucía, CSIC, Granada, Spain,
717 the Scientific Support Office of the European Space Agency, Noordwijk, The Netherlands, the
718 Instituto Nacional de Técnica Aeroespacial, Madrid, Spain, the Universidad Politécnica de Madrid,
719 Spain, the Department of Physics and Astronomy of Uppsala University, Sweden, and the Institut für
720 Datentechnik und Kommunikationsnetze der Technischen Universität Braunschweig, Germany.
721

722 **References**

723

724 El-Maarry, M. R., and 53 colleagues, (2015), Regional surface morphology of comet 67P/Churyumov-
725 Gerasimenko from Rosetta/OSIRIS images, *Astronomy and Astrophysics*, 583, A26,
726 doi:10.1051/0004-6361/201525723.

727

728 El-Maarry, M. R., and 51 colleagues, (2016), Regional surface morphology of comet 67P/Churyumov-
729 Gerasimenko from Rosetta/OSIRIS images: The southern hemisphere, *Astronomy and Astrophysics*,
730 593, A110.

731

732 El-Maarry, M. R., and 51 colleagues, (2017a), Regional surface morphology of comet
733 67P/Churyumov-Gerasimenko from Rosetta/OSIRIS images: The southern hemisphere
734 (Corrigendum), *Astronomy and Astrophysics*, 598, C2.

735

736 El-Maarry, M. R., and 55 colleagues, (2017b), Surface changes on comet 67P/Churyumov-
737 Gerasimenko suggest a more active past, *Science*, 355, 1392-1395.

738

739 Fornasier, S., and 53 colleagues, (2017), The highly active Anhur-Bes regions in the 67P/Churyumov-
740 Gerasimenko comet: results from OSIRIS/ROSETTA observations, *Monthly Notices of the Royal*
741 *Astronomical Society*, 469, S93-S107.

742

743 Ip, W.-H., and 54 colleagues, (2016), Physical properties and dynamical relation of the circular
744 depressions on comet 67P/Churyumov-Gerasimenko, *Astronomy and Astrophysics*, 591, A132.

745

746 Jorda, L., R. Gaskell, C. Capanna, S. Hviid, P. Lamy, J. Durech, G. Faury, O. Groussin, P. Gutiérrez, C.
747 Jackman, S. J. Keihm, H. U. Keller, J. Knollenberg, E. Kuehrt, S. Marchi, S. Mottola, E. Palmer, F. P.
748 Schloerb, H. Sierks, J.-B. Vincent, M. F. A'Hearn, C. Barbieri, R. Rodrigo, D. Koschny, H. Rickman, M. A.
749 Barucci, J. L. Bertaux, I. Bertini, G. Cremonese, V. Da Deppo, B. Davidsson, S. Debei, M. De Cecco, S.
750 Fornasier, M. Fulle, C. Guettler, W.-H. Ip, J. R. Kramm, M. Kueppers, L. M. Lara, M. Lazzarin, J. J.
751 Lopez Moreno, F. Marzari, G. Naletto, N. Ockay, N. Thomas, C. Tubiana, and K.-P. Wenzel, (2016), The
752 global shape, density and rotation of Comet 67P/Churyumov-Gerasimenko from preperihelion
753 Rosetta/OSIRIS observations, *Icarus*, 277, 257-278.

754

755 Keller, H. U., S. Mottola, S. F. Hviid, J. Agarwal, E. Kuehrt, Y. Skorov, K. Otto, J.-B. Vincent, N. Ockay, S.
756 E. Schröder, B. Davidsson, M. Pajola, X. Shi, D. Bodewits, I. Toth, F. Preusker, F. Scholten, H. Sierks, C.
757 Barbieri, P. Lamy, R. Rodrigo, D. Koschny, H. Rickman, M. F. A'Hearn, M. A. Barucci, J.-L. Bertaux, I.
758 Bertini, G. Cremonese, V. Da Deppo, S. Debei, M. De Cecco, J. Deller, S. Fornasier, M. Fulle, O.
759 Groussin, P. J. Gutiérrez, C. Güttler, M. Hofmann, W.-H. Ip, L. Jorda, J. Knollenberg, J. R. Kramm, M.
760 Küppers, L.-M. Lara, M. Lazzarin, J. J. Lopez-Moreno, F. Marzari, G. Naletto, C. Tubiana, and N.
761 Thomas, (2017), Seasonal mass transfer on the nucleus of comet 67P/Churyumov-Gerasimenko,
762 *Monthly Notices of the Royal Astronomical Society*, 469, S357-S371.

763

764 Lavoué, G. (2009) A Local Roughness Measure for 3D Meshes and Its Application to Visual Masking,
765 *ACM Transactions on Applied Perception*, 5(4), 21:1-21:23.

766

767 Preusker, F., F. Scholten, K.-D. Matz, T. Roatsch, K. Willner, S. F. Hviid, J. Knollenberg, L. Jorda, P. J.
768 Gutiérrez, E. Kuehrt, S. Mottola, M. F. A'Hearn, N. Thomas, H. Sierks, C. Barbieri, P. Lamy, R. Rodrigo,
769 D. Koschny, H. Rickman, H. U. Keller, J. Agarwal, M. A. Barucci, J.-L. Bertaux, I. Bertini, G. Cremonese,
770 V. Da Deppo, B. Davidsson, S. Debei, M. De Cecco, S. Fornasier, M. Fulle, O. Groussin, C. Güttler, W.-
771 H. Ip, J. R. Kramm, M. Küppers, L. M. Lara, M. Lazzarin, J. J. Lopez-Moreno, F. Marzari, H. Michalik, G.
772 Naletto, N. Ockay, C. Tubiana, and J.-B. Vincent, (2015), Shape model, reference system definition,

- 773 and cartographic mapping standards for comet 67P/Churyumov-Gerasimenko - Stereo-
774 photogrammetric analysis of Rosetta/OSIRIS image data, *Astronomy and Astrophysics*, 583, A33.
- 775 Preusker, F., F. Scholten, K.-D. Matz, T. Roatsch, S. F. Hviid, S. Mottola, J. Knollenberg, E. Kührt,
776 M. Pajola, N. Ockay, J.-B. Vincent, B. Davidsson, M. F. A'Hearn, J. Agarwal, C. Barbieri, M. A.
777 Barucci, J.-L. Bertaux, I. Bertini, G. Cremonese, V. Da Deppo, S. Debei, M. De Cecco, S. Fornasier,
778 M. Fulle, O. Groussin, P. J. Gutiérrez, C. Güttler, W.-H. Ip, L. Jorda, H. U. Keller, D. Koschny, J. R.
779 Kramm, M. Küppers, P. Lamy, L. M. Lara, M. Lazzarin, J. J. Lopez Moreno, F. Marzari, M.
780 Massironi, G. Naletto, H. Rickman, R. Rodrigo, H. Sierks, N. Thomas, and C. Tubiana, (2017),
781 *Astron. Astrophys.*, 607, L1, DOI: 10.1051/0004-6361/201731798.
- 782 Sierks, H., C. Barbieri, P.L. Lamy, R. Rodrigo, D. Koschny, H. Rickman, H.U. Keller, J. Agarwal, M.F.
783 A'Hearn, F. Angrilli, A.-T. Auger, M.A. Barucci, J.-L. Bertaux, I. Bertini, S. Besse, D. Bodewits, C.
784 Capanna, G. Cremonese, V. Da Deppo, B. Davidsson, S. Debei, M. De Cecco, F. Ferri, S. Fornasier, M.
785 Fulle, R. Gaskell, L. Giacomini, O. Groussin, P. Gutierrez-Marques, P.J. Gutiérrez, C. Güttler, N.
786 Hoekzema, S.F. Hviid, W.-H. Ip, L. Jorda, J. Knollenberg, G. Kovacs, J.-R. Kramm, E. Kührt, M. Küppers,
787 F. La Forgia, L.M. Lara, M. Lazzarin, C. Leyrat, J.J. Lopez Moreno, S. Magrin, S. Marchi, F. Marzari, M.
788 Massironi, H. Michalik, R. Moissl, S. Mottola, G. Naletto, N. Ockay, M. Pajola, M. Pertile, F. Preusker,
789 L. Sabau, F. Scholten, C. Snodgrass, N. Thomas, C. Tubiana, J.-B. Vincent, K.-P. Wenzel, M.
790 Zaccariotto, M. Pätzold, (2015), On the nucleus structure and activity of comet 67P/Churyumov-
791 Gerasimenko, *Science*, 347, aaa1044, 23 January 2015.
- 792 Thomas, N., H. Sierks, C. Barbieri, P.L. Lamy, R. Rodrigo, H. Rickman, D. Koschny, H.U. Keller, J.
793 Agarwal, M.F. A'Hearn, F. Angrilli, A.-T. Auger, M.A. Barucci, J.-L. Bertaux, I. Bertini, S. Besse, D.
794 Bodewits, G. Cremonese, V. Da Deppo, B. Davidsson, M. De Cecco, S. Debei, M.-R. El-Maarry, F. Ferri,
795 S. Fornasier, M. Fulle, L. Giacomini, O. Groussin, P.J. Gutierrez, C. Güttler, S.F. Hviid, W.-H. Ip, L.
796 Jorda, J. Knollenberg, J.-R. Kramm, E. Kührt, M. Küppers, F. La Forgia, L.M. Lara, M. Lazzarin, J.J.
797 Lopez Moreno, S. Magrin, S. Marchi, F. Marzari, M. Massironi, H. Michalik, R. Moissl, S. Mottola, G.
798 Naletto, N. Ockay, M. Pajola, A. Pommerol, F. Preusker, L. Sabau, F. Scholten, C. Snodgrass, C.
799 Tubiana, J.-B. Vincent, K.-P. Wenzel (2015), The Morphological Diversity of Comet 67P/Churyumov-
800 Gerasimenko, *Science*, 347, aaa0440, 23 January 2015.
- 801 Thomas, N., B. Davidsson, M.R. El-Maarry, S. Fornasier, L. Giacomini, A.G. Gracia Berna, S.F. Hviid,
802 W.-H. Ip, L. Jorda, H.U. Keller, J. Knollenberg, E. Kührt, F. La Forgia, I.L. Lai, Y. Liao, R. Marschall, M.
803 Massironi, S. Mottola, M. Pajola, O. Poch, A. Pommerol, F. Preusker, F. Scholten, C.C. Su, J.S. Wu, J.-
804 B. Vincent, H. Sierks, C. Barbieri, P.L. Lamy, R. Rodrigo, H. Rickman, D. Koschny, M.F. A'Hearn, M.A.
805 Barucci, J.-L. Bertaux, I. Bertini, G. Cremonese, V. Da Deppo, S. Debei, M. Fulle, O. Groussin, P.J.
806 Gutierrez, J.-R. Kramm, M. Küppers, L. M. Lara, M. Lazzarin, J. J. Lopez Moreno, F. Marzari, H.
807 Michalik, G. Naletto, and C. Güttler, (2015), Redistribution of particles across the nucleus of comet
808 67P/Churyumov-Gerasimenko, *Astron. Astrophys.*, 583, A17, dx.doi:10.1051/0004-6361/201526049.
- 809 Vincent, J.-B., and 66 colleagues (2015), Large heterogeneities in comet 67P as revealed by active
810 pits from sinkhole collapse, *Nature*, 523, 63-66.
- 811 Vincent, J.-B., and 54 colleagues, (2016), Are fractured cliffs the source of cometary dust jets?
812 Insights from OSIRIS/Rosetta at 67P/Churyumov-Gerasimenko, *Astronomy and Astrophysics*, 587,
813 A14.

814

815 **Figures**

816 Figure 1 Montage of 4 orientations of the nucleus of 67P showing the region definitions (Thomas
817 et al., 2015; El-Maarry et al., 2015;2016) on the SHAP7 model. 10

818 Figure 2 Left: OSIRIS image (NAC_2015-12-10T05.01.06.778Z_ID10_1397549000_F22) showing
819 the Anubis-Atum-Khonsu face on the body and the Anuket-Neith-Sobek section on the head. Right:
820 The regional definition on the shape model with sub-regions added in the same orientation as the
821 image..... 11

822 Figure 3 Left: The Khonsu face of the nucleus (NAC_2015-05-
823 02T15.09.20.389Z_ID10_1397549000_F23). Right: The sub-region definition of Khonsu. 12

824 Figure 4 Left: OSIRIS image (NAC_2015-12-18T03.43.20) showing the Khonsu region and its
825 relationship to Atum (particularly sub-region a) and Apis. 13

826 Figure 5 Left: OSIRIS image NAC_2014-12-02T07.59.13.739Z_ID10_1397549001_F23 showing
827 the edge defining the interface between Ash and Babi. The shape model (right) shows sub-region a
828 in yellow. The hummocky interface to sub-region c (purple) is also visible..... 13

829 Figure 6 Left: OSIRIS image NAC_2014-08-16T18.59.14. Right: The corresponding sub-region
830 definition. Note the positions of the Aker sub-regions and their relationship to the two sub-regions
831 of Babi. Note also the sub-regions of Ash..... 14

832 Figure 7 Left: OSIRIS image NAC_2015-05-11T20.29.18 Right: The sub-region definition. Note the
833 circular structure defined as Ash sub-region e and the Seth-like part of Ash, sub-region g. 15

834 Figure 8 Left: OSIRIS image NAC_2014-09-02T12.44.22. Right: The sub-region definition. Apis and
835 Atum show much reduced dust-coverage compared to Ash while the Ash sub-regions show different
836 topography. Note the presence of layering in sub-region i..... 15

837 Figure 9 Left: OSIRIS image NAC_2015-05-11T13.07.42. Right: The sub-region definition showing
838 Aten at the centre of the body in this view. Note the brown coloured sub-region (Ash j) which is a
839 dust-covered depression (but much shallower than Aten). 15

840 Figure 10 Left: OSIRIS image NAC_2014-11-22T10.52.53.805Z_ID10_1397549000_F22. Right: The

841 sub-region definition showing in particular the face of Aker leading down to the Hapi region in the

842 neck..... 16

843 Figure 11 Left: OSIRIS image NAC_2015-04-29T17.24.09. Right: The sub-region definition for

844 Imhotep..... 17

845 Figure 12 View of the 3D shape model which emphasizes the topographic differences within the

846 Imhotep region. The relationships of Imhotep (sub-regions a-c) to Ash and Apis are also well brought

847 out in this view. The Bes sub-regions (a-e) are also evident on the left of the diagram. Two sub-

848 regions (i and j) of Ash are marked..... 17

849 Figure 13 Left: OSIRIS image NAC_2015-08-01T13.51.57. Right: The sub-region definition. Anhur

850 sub-region a (light blue) is bounded by the cliff (Anhur sub-region b) that descends into the neck.

851 Note that Anhur sub-region c (green) has similar topographical properties to the Geb region..... 18

852 Figure 14 The shape model oriented to show clearly the topographic relationships between the

853 different sub-regions of Anhur and the Geb region. The topographical relations within Wosret are

854 also well-seen in this view. Other major sub-regions are marked. 18

855 Figure 16 OSIRIS image acquired on 2 Jan 2016 at 06:28:42 showing sub-region a of Geb. The

856 flat, smooth region above it is Anubis. The cliff of Geb is highly fractured and pitted. 19

857 Figure 16 The Bes and Imhotep sub-region definition. Left: OSIRIS image NAC_2015-08-

858 01T23.55.10. Right: The 3D shape model. Bes mostly covers one long, thin face of the body of the

859 nucleus with different topographical layers delineated by steep cliffs..... 20

860 Figure 17 Left: OSIRIS image NAC_2016-01-30T10.41.49.690Z_ID10_1397549900_F22. Right: The

861 sub-region definition. The stepped structure of Sobek is evident at the centre of the image. 21

862 Figure 18 Left: OSIRIS image NAC_2016-01-02T17.23.24.646Z_ID10_1397549300_F22. Right: The

863 sub-region definition. The Wosret region is particularly interesting in this image. The image shows

864 the topographic and textural differences that have led to the definition of 3 sub-regions..... 22

865 Figure 19 Left: OSIRIS image NAC_2014-08-06T01.19.14. Right: The sub-region definition
866 showing the nucleus along its long axis with Hatmehit in the foreground. 23

867 Figure 20 Left: OSIRIS image NAC_2015-03-05T00.38.41.069Z_ID10_1397549003_F41. Right: The
868 sub-region definition showing Serqet in the centre of the image. Ma'at sub-regions a and b are also
869 evident to the right of Serqet. The Hatmehit sub-regions (a, b, and c) are also marked. 24

870 Figure 21 The shape model showing the 5 sub-regions of Maat. Note the different surface
871 appearances. 25

872 Figure 22 A quantitative expression of the roughness of the Apis and Hapi regions on the
873 nucleus. The y-axis expresses the normalized area in each bin. The x axis defines the effective
874 curvature difference between the original object and a smoothed version of that object with a scale
875 parameter equal to 20 m. 28

876 Figure 23 As Figure 22 but for the Anhur and Sobek regions. Notice that the distribution is much
877 broader indicating a large distribution of roughness. The peak of the distribution is also shifted to
878 higher roughness values. 29

879

Highlights

- Regions are defined upon the latest 3D shape model (SHAP7) of comet 67P/Churyumov-Gerasimenko.
- The definition is provided in a publicly accessible shape file.
- Sub-regions of similar properties are defined to support more detailed work.
- Roughness calculations are performed to quantify differences between regions and sub-regions.